NATURE RED TOOTH AND CLAW: STUDIES OF EXTINCT AND EXTANT ARTHROPOD PREDATOR-PREY SYSTEMS

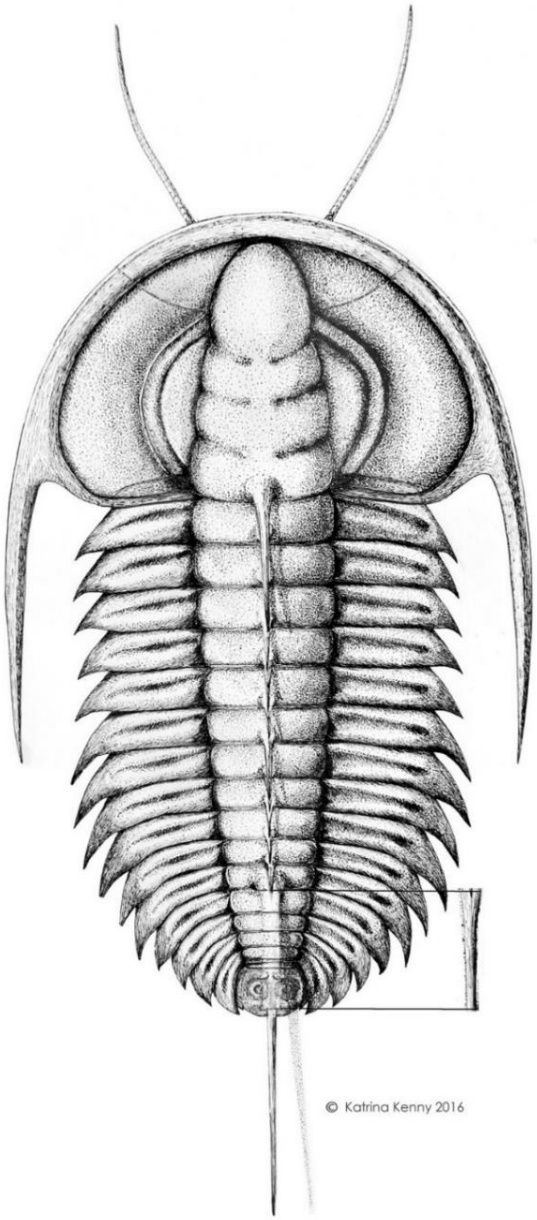

Reconstruction of Redlichia takooensis *from the lower Cambrian Emu Bay Shale. Illustration by K. Kenny.*

Russell Dean Christopher Bicknell

BSc, MSc, GradDipSci (Victoria University of Wellington)

Palaeoscience Research Centre, University of New England, Armidale, Australia

Thesis presented for the degree of Doctor of Philosophy, 12th April 2019.

Gutta cavat lapidem, non vi, sed sæpe cadendo.

Lucretius

STATEMENT OF CANDIDATE

I certify that the work in this thesis entitled "*Nature red tooth and claw: Studies of extinct and extant arthropod predator-prey systems*" has not previously been submitted for a degree, nor has it been submitted as part of requirements for a degree to any other university or institution other than the University of New England, Armidale. I also certify that the thesis is an original piece of research and any assistance that I have received in the preparation thereof has been appropriately acknowledged.

Russell D. C. Bicknell

12th April, 2019

ACKNOWLEDGEMENTS

Over the past three years I have been supported, prompted, coaxed, and pushed to publish this research by many people. It is therefore with great privilege that I humbly thank those people who helped me get this thesis over the line.

To my UNE crew: Researchers at the University of New England's Palaeoscience Research Centre are some of the most amazing academics I have ever met. Over the past three years I have been helped, challenged, talked into and out of ideas, and have ultimately been made a better academic for it. I thank Ada Klinkhamer, Lachlan Hart, Justin Ledogar, Marissa Betts, Rex Mitchell, Rudy Lerosey-Aubril, and Tom Brougham for help, words, drinks and edits.

A special mention goes to Nicolás Campione. Nic has spent countless hours with me drinking coffee and/or beer while copping a barrage of questions relating to topics rather left-field of his corner of palaeontology. He helped me find angles to my work that I could not see and has made me a much more successful academic in doing so. To this end, I thank him for being an amazing friend, colleague, and the mentor I did not know I needed (and thank you for always correcting my lack of Oxford commas!).

To the academics across the globe: The past three years resulted in collaborations with researchers across both Australia and abroad. As such, I thank Glenn Brock, James Holmes, Diego García-Bellido, Patrick Smith, and Richard Flavel (Australia), Jean-Bernard Caron, and David Rudkin (Canada), Samuel Zamora (Spain), Christian Skovsted (Sweden), Allison Daley (Switzerland), David Legg, Greg Edgecombe, Harriet Drage, and Lyall Anderson (UK), Allan Lerner, Ben Gutzler, Javier Ortega-Hernandez, Mark Botton, and Win Watson III (USA) for all the help, support, advice, and the countless emails you have had to deal with.

Special thanks is given to Stephen Pates. There are no words that can articulate how much I appreciate you, my friend. The collaboration we have built over the past three years has been so very fruitful and working with you is always fun. Thank you for your constant willingness to read my work and improve it with your own 'Pates-ie' flare.

To the curators and museum managers: The research conducted here would not have been possible without the help of curatorial staff. I must therefore thank Paul Mayer (Field Museum of Natural History, Chicago, Illinois, USA), Mark Webster (Institute for Cambrian Studies, University of Chicago, Chicago, Illinois, USA), Mark Carnall (Oxford Museum of Natural History), Maryam Akrami (Royal Ontario Museum. Toronto, Canada), Jessica Cundiff (Museum of Comparative Zoology, Harvard, Boston, Massachusetts, USA), Mary-Anne Binnie (South Australian Museum, Adelaide, South Australia, Australia), Susan Butts, Jessica Utrup, Lourdes Rojas (Yale Peabody Museum, New Haven, Connecticut, USA), and Mark Florence (National Museum of Natural History, Washington, DC, USA) for their help with collections across the globe. It is fair to say that my work would not have been possible without you and your dedication to research.

To my non-academic crew: You are the friends who supported me over the past three years. The people who bought me coffee, beer, and scotch. Who listened to me brag and complain. Who revelled in the highlights and commiserated in the lowlights. To this end, I thank my closest friends Dana Morrison, Morgan "Dance" Fisher, Rachel Skudder, Miriam Khan, and Tanya Simmons for always offering help and support. Special thanks are given to Luke "Paddock" Field and Dylan "Smiddty" Smith for the beers/scotch/gin/goon/whatever else we have consumed over the past years. My liver might not thank you, but I do.

To my family: I thank my family for supporting my choices to move to Australia and follow my passions. Without their support I am not certain I would be here today.

To Steve Wroe: As a researcher who focuses primarily on vertebrates, I feel like I dropped you in the deep-end talking about these animals that have skeletons on the outside. But without your supervision, support, and new ideas, I would not have achieved nearly as much as I have. So thank you for putting up with my lists of silly questions (e.g., "what is the difference between stress and strain?") and helping push out my research to the world.

To John Paterson: Not everyone would take on a student from another country, especially when all you know of them is via emails! But you did. And your penance for this has been three years of questions, annoying interruptions, and a host of subpar manuscripts that probably drove you to the bottle. For this I cannot thank you enough. Working under you, learning from you, and having you push me to do my own research was unarguably central in me becoming the academic I am and will continue to be. Thank you for the weekends you spent editing my work, the time you took to explain to me the nuances of being a scientist, the stupid in-jokes ("is it brain or not brain?!"), and the yarns we had. This candidature has been made so much more fun for these experiences.

DEDICATION

This work is dedicated to my parents for supporting my choice to follow my dreams and to Prof. John R. Paterson for guiding me during my candidature.

PREFACE

The work presented herein is the result of a thesis by publication. As such, all chapters except the Introduction and Conclusion are presented as the journal-formatted publications that have been subject to peer-review and deemed acceptable for publication by the journal editorial staff.

TABLE OF CONTENTS

ABSTRACT

Records of Cambrian predation have long been recognised as unequivocal evidence for the earliest predator-prey systems. However, Cambrian predation has been somewhat poorly documented in a numerical and comparative context – a problem rectified in this thesis. The first quantitative, model-based evidence illustrating how effective Cambrian predators were at shell crushing is presented. The modern day horseshoe crab is used to understand how Cambrian prey responded to attacks. Finally, the previously purported right-side injury bias observed on Cambrian trilobites is redressed using single fossil deposits and single species – this approach reveals no right-side bias.

INTRODUCTION

Background and Objectives

The Cambrian Explosion is the most rapid and stunning biological diversification event in the fossil record: a revolution that resulted in rise of animals and complex marine ecosystems (Erwin et al., 2011; Budd & Jensen, 2017). Two hallmarks of the Explosion are: (1) the evolution of prey organisms bearing biomineralised shells and exoskeletons, and (2) the rise of predatory tool kits needed to effectively capitalise on these prey (Vermeij, 1989; Bengtson, 2002; Babcock, 2003; Leighton, 2011; Budd & Mann, 2019). As such, the Cambrian saw the first definite examples of shell-crushing (durophagy) and shell-drilling interactions. Despite the extensive record of Cambrian shelly predation, few studies have examined collections of biomineralised Cambrian organisms to explore predation patterns (e.g., Babcock, 1993; Conway Morris and Bengtson, 1994; Vendrasco et al., 2011). Furthermore, prior to this thesis, no peer-reviewed studies had quantitatively explored the supposed shell-crushing ability of Cambrian durophages, specifically arthropods with gnathobases (teeth-like spines on various appendages). This thesis addresses these two topics using three objectives:

1) Develop methods for exploring the durophagous ability of gnathobase-bearing Cambrian arthropods using *Limulus polyphemus*, the iconic American horseshoe crab, as a modern analogue.
2) Study exoskeletal abnormalities in horseshoe crabs to understand injury morphologies and compare them to possible injuries in Cambrian trilobites; this develops on suggestions made by Jell (1989).
3) Quantitatively explore records of trilobite injuries in single fossil deposits to uncover patterns and redress a central topic in Cambrian predation research: lateralisation in trilobite defences and predatory behaviour.

I present eight peer-reviewed and published works that thoroughly explored these objectives.

Review of Cambrian predation (Paper 1)

Shelly predation in the Cambrian is a well-documented topic (McMenamin, 1987; Bengtson, 1994, 2002; Butterfield, 2001; Leighton, 2011). However, a systematic summary of all evidence for Cambrian-aged shelly predation has never been presented. To grasp the scope of this topic, and indeed my thesis, I present a review that synthesised the literature on the topic, documenting all known examples of Cambrian-aged injuries, drill holes, coprolites, and gut contents (cololites). The examples presented in this paper have since been expanded upon in more recent publications (e.g., Daley et al., 2018; Kimmig & Pratt, 2018; Lerosey-Aubril & Peel, 2018; Zhang & Brock, 2018). The review also explored plausible Cambrian predators and highlighted that biomechanical analyses (see Paper 4) are needed to fully understand the ability of these groups.

Cambrian predators and biomechanics (Papers 2–4)

Sidneyia inexpectans—a gnathobase-bearing artiopodan arthropod—is an iconic taxon from the middle Cambrian Burgess Shale. *Sidneyia inexpectans* cololites containing fragmented trilobites and brachiopods suggest that the organism was a durophagous predator and used gnathobases on its walking legs to crush and consume prey, similar to *Limulus polyphemus* (Bruton, 1981; Zacaï et al., 2016). However, this hypothesis has not been tested biomechanically. Papers 2–4 present three steps toward confirming the idea outlined in Bruton (1981) and Zacaï et al. (2016). Paper 2 compared the cuticular microstructure of gnathobases from three taxa: *L. polyphemus* (a known durophage), plus *Eurypterus tetragonophthalmus* (a Silurian eurypterid) and *S. inexpectans*, both possible durophages. This work highlighted that *L. polyphemus* and *S. inexpectans* gnathobases are microstructurally similar, supporting the shell-crushing ability of the latter species. Papers 3

and 4 developed the use of micro-computer tomography (micro-CT) scans and 3D reconstructions of organisms to further explore the durophagous ability of *S. inexpectans*. Paper 3 presented the first 3D atlas of *L. polyphemus* using CT and micro-CT scans. Furthermore, iodine-staining of specimens, following Gignac & Kley (2014) and Gignac et al. (2016) , allowed for the first documentation of *L. polyphemus* muscles *in situ*: an approach employed for gathering the necessary muscle data used in Paper 4. Paper 3 has since been cited in reviews on 3D reconstructions in biology (Newe & Becker, 2018; Semple et al., 2019). Paper 4 used 3D Finite Element Analysis (FEA) to compare the mechanical advantage of *L. polyphemus* and *S. inexpectans*. Results show that, as Paper 2 suggested, *S. inexpectans* was an effective shell crusher, highlighting the origin of effective gnathobasic durophagous predation in the Cambrian.

Modern abnormalities and Cambrian injuries (Papers 5 and 6)

Jell (1989) suggested that abnormalities observed on extant arthropods may help explain how injuries observed on fossils may have developed. To expand on this hypothesis, Papers 5 and 6 assessed abnormal horseshoe crab specimens and used these data to suggest how Cambrian trilobite abnormalities may have developed during the soft-shelled stages trilobites experienced post-moult. Furthermore, these papers developed on the limited data concerning abnormal extinct and extant horseshoe crabs (see van der Meer Mohr, 1935; Shuster Jr., 1982; Jell, 1989). Paper 5 highlighted that extreme ‘W’-shaped cephalothoracic injuries on horseshoe crabs are similar to cephalic injuries on Cambrian trilobites. This comparison confirmed that at least ‘W’-shaped injuries on Cambrian trilobites occurred after a moulting event. Paper 6 expanded on Paper 5 to consider all extant horseshoe crab species. A rare example of a horseshoe crab with two moveable thoracetronic spines recovering from the same spine embayment was compared to Cambrian trilobites with two thoracic spines

recovering from the same thoracic section. This comparison showed that such thoracic abnormalities resulted from injuries and abnormal recovery.

Trilobite injuries from single deposits (Papers 7 and 8)

Cambrian trilobite injury patterns were previously assessed by Babcock and Robison (1989) and Babcock (1993). Their dataset, which was a compilation of injured specimens from multiple Cambrian fossil deposits, suggested that Cambrian trilobite injuries were most often located on the posterior and right-side of the exoskeleton. These results were used to assert that Cambrian predators had lateralised attack strategies and/or that trilobite prey had lateralised defence strategies. Papers 7 and 8 reconsidered this concept by assessing injury patterns on trilobite taxa from two distinct Cambrian-aged deposits. The major differences between Babcock's (1993) study and Papers 7 and 8 were (1) the use of advanced statistical methods, and (2) a concerted effort to treat deposits as closed systems and not lump data from various sites with disparate ages. Paper 7 showed, among other interesting results, that there was no evidence for lateralisation in injuries to *Eccaparadoxides pradoanus* specimens from the Huérmeda Formation (Cambrian Series 2, Stage 4) in Spain. These data also showed that injuries are located most commonly on the posterior part of the thorax. Paper 8 examined olenelline trilobites from the Ruin Wash *Lagerstätte* (Cambrian Series 2, Stage 4) in Nevada, USA, reaffirming that lateralised injuries were not observed when considering taxa in isolation, and that injuries to the posterior exoskeleton were common. Paper 8 also presented the first thorough consideration of how thoracic spines may have deterred predatory attacks.

Supplementary Papers (9-12)

[Note to Examiners: These supplementary papers represent non-thesis-related research contributions published during candidature. Thus, they should not be assessed as part of the

PhD thesis. They are included to demonstrate the breadth of skills employed by the candidate and his eagerness to make contributions across the natural and quantitative sciences.]

The supplementary papers emphasise two distinct aspects of research that interest the candidate: (1) the use of cuticular microstructural features to understand evolutionary or form-function relationships between taxa; and (2) the use of geometric morphometrics (also considered in Paper 7) to uncover populations, explore evolutionary stories, and augment taxonomy.

Microstructure of cuticular features in arthropods has been relatively well documented (Neville, 1975; Dalingwater, 1987), but Paper 2 (discussed above) highlighted that select exoskeletal parts have received less attention than others. The microstructure of arthropod mandibles, specifically ants, is one such area. Supplementary Paper 9 considered the mandible microstructure of four Australian ant taxa to show a highly conserved morphology and a possible example of evolutionary stasis at a microscopic scale.

The field of geometric morphometrics (GM) gave biology and palaeontology an ideal avenue to quantitatively explore evolution, population variation, and even taxonomy (Adams et al., 2004, 2013; Zelditch et al., 2004; Slice, 2007; Lawing & Polly, 2010). Three papers, in addition to Paper 7, were produced to thoroughly explore the uses of this tool (Supplementary Papers 10–12). Supplementary Paper 10 used GM to show that specimens of the enigmatic Ediacaran organism *Parvancorina minchami* from the Flinders Ranges, South Australia were all from the same population. Supplementary Paper 11 used GM to explore the evolutionary history of the foraminifera *Truncorotalia* across the Miocene-Pliocene boundary. The application showed the first plausible example of quantum evolution among planktonic foraminifera. Supplementary Paper 12 used GM in a novel way to support the erection of a new Triassic-aged horseshoe crab genus and species: *Sloveniolimulus rudkini*. This same

work also highlighted the high diversity and disparity of horseshoe crabs after the end-Permian extinction.

ESTIMATED PROPORTION OF CONTRIBUTIONS TO PAPERS

Papers	Extent of intellectual input by candidate (%)				
	Study concept and design	Data acquisition	Data analysis and interpretation	Manuscript drafting	Critical revision
Reappraising the early evidence of durophagy and drilling predation in the fossil record: implications for escalation and the Cambrian Explosion	80	90	80	80	85
The gnathobasic spine microstructure of recent and Silurian chelicerates and the Cambrian artiopodan *Sidneyia*: Functional and evolutionary implications	100	80	90	90	85
A 3D anatomical atlas of appendage musculature in the chelicerate arthropod *Limulus polyphemus*	80	90	85	90	85
Computational biomechanical analyses demonstrate similar shell-crushing abilities in modern and ancient arthropods	80	70	80	85	85
Abnormal xiphosurids, with possible application to Cambrian trilobites	100	85	90	90	90
Abnormal extant xiphosurids in the Yale Peabody Museum Invertebrate Zoology collection	100	95	95	90	90

Quantitative analysis of repaired and unrepaired damage to trilobites from the Cambrian (Stage 4, Drumian) Iberian Chains, NE Spain (co-authored)	40	40	50	30	85
Elongated thoracic spines as predatory deterrents in olenelline trilobites from the lower Cambrian of Nevada (co-authored)	30	30	60	50	85

References

Adams, D. C., Rohlf, F. J., & Slice, D. E. (2004). Geometric morphometrics: ten years of progress following the 'revolution'. *Italian Journal of Zoology, 71*, 5–16.

Adams, D. C., Rohlf, F. J., & Slice, D. E. (2013). A field comes of age: Geometric morphometrics in the 21st century. *Hystrix, 24*, 7–14.

Babcock, L. E. (1993). Trilobite malformations and the fossil record of behavioral asymmetry. *Journal of Paleontology, 67*, 217–229.

Babcock, L. E. (2003). Trilobites in Paleozoic predator-prey systems, and their role in reorganization of early Paleozoic ecosystems. In P. Kelley, M. Kowalewski, & T. A. Hansen (Eds.), *Predator—prey interactions in the fossil record* (pp. 55–92). New York: Plenum Publishers.

Babcock, L. E., & Robison, R. A. (1989). Preferences of Palaeozoic predators. *Nature, 337*, 695–696.

Bengtson, S. (1994). The advent of animal skeletons. In *Early Life on Earth: Nobel Symposium, No. 84* (pp. 412–425). New York: Columbia University Press.

Bengtson, S. (2002). Origins and early evolution of predation. *Paleontological Society Papers, 8*, 289–318.

Bruton, D. L. (1981). The arthropod *Sidneyia inexpectans*, Middle Cambrian, Burgess Shale, British Columbia. *Philosophical Transactions of the Royal Society of London. Series B, Biological Sciences, 295*, 619–653.

Budd, G., & Mann, R. P. (2019). Modeling durophagous predation and mortality rates from the fossil record of gastropods. *Paleobiology*, 1–19. doi:10.1017/pab.2019.1012.

Budd, G. E., & Jensen, S. (2017). The origin of the animals and a 'Savannah' hypothesis for early bilaterian evolution. *Biological Reviews, 92*, 446–473.

Butterfield, N. J. (2001). Cambrian food webs. In D. E. G. Briggs & P. R. Crowther (Eds.), *Paleobiology II* (pp. 40–43). Oxford: Blackwell Publishing.

Conway Morris, S., & Bengtson, S. (1994). Cambrian predators: possible evidence from boreholes. *Journal of Paleontology, 68*, 1–23.

Daley, A. C., Antcliffe, J. B., Drage, H. B., & Pates, S. (2018). Early fossil record of Euarthropoda and the Cambrian Explosion. *Proceedings of the National Academy of Sciences, 115*, 5323–5331.

Dalingwater, J. E. (1987). Chelicerate cuticle structure. In W. Nentwig (Ed.), *Ecophysiology of Spiders* (pp. 3–15). Berlin: Springer.

Erwin, D. H., Laflamme, M., Tweedt, S. M., Sperling, E. A., Pisani, D., & Peterson, K. J. (2011). The Cambrian conundrum: early divergence and later ecological success in the early history of animals. *Science, 334*, 1091–1097.

Gignac, P. M., & Kley, N. J. (2014). Iodine-enhanced micro-CT imaging: Methodological refinements for the study of the soft-tissue anatomy of post-embryonic vertebrates. *Journal of Experimental Zoology (Molecular and Developmental Evolution), 322B*, 166–176.

Gignac, P. M., Kley, N. J., Clarke, J. A., Colbert, M. W., Morhardt, A. C., Cerio, D., . . . Witmer, L. M. (2016). Diffusible iodine-based contrast-enhanced computed

tomography (diceCT): an emerging tool for rapid, high-resolution, 3-D imaging of metazoan soft tissues. *Journal of Anatomy, 228*, 889–909.

Jell, P. A. (1989). Some aberrant exoskeletons from fossil and living arthropods. *Memoirs of the Queensland Museum, 27*, 491–498.

Kimmig, J., & Pratt, B. R. (2018). Coprolites in the Ravens Throat River Lagerstätte of northwestern Canada: implications for the middle Cambrian food web. *Palaios, 33*, 125–140.

Lawing, A. M., & Polly, P. D. (2010). Geometric morphometrics: recent applications to the study of evolution and development. *Journal of Zoology, 280*, 1–7.

Leighton, L. R. (2011). Analyzing predation from the Dawn of the Phanerozoic. In M. Laflamme, J. D. Schiffbauer, & S. Q. Dornbos (Eds.), *Quantifying the Evolution of Early Life* (pp. 73–109). Dordrecht: Springer.

Lerosey-Aubril, R., & Peel, J. S. (2018). Gut evolution in early Cambrian trilobites and the origin of predation on infaunal macroinvertebrates: evidence from muscle scars in *Mesolenellus*. *Palaeontology, 61*, 747–760.

McMenamin, M. A. S. (1987). The emergence of animals. *Scientific American, 256*, 94–102.

Neville, A. C. (1975). *Biology of the Arthropod Cuticle* (Vol. 4). New York: Springer Verlag.

Newe, A., & Becker, L. (2018). Three-dimensional portable document format (3D PDF) in clinical communication and biomedical sciences: Systematic review of applications, tools, and protocols. *JMIR Medical Informatics, 6*, e10295.

Semple, T. L., Peakall, R., & Tatarnic, N. J. (2019). A comprehensive and user-friendly framework for 3D-data visualisation in invertebrates and other organisms. *Journal of Morphology, 280*, 223–231.

Shuster Jr., C. N. (1982). A pictorial review of the natural history and ecology of the horseshoe crab *Limulus polyphemus*, with reference to other Limulidae. *Progress in Clinical and Biological Research, 81*, 1–52.

Slice, D. E. (2007). Geometric morphometrics. *Annual Review of Anthropology, 36*, 261–281.

van der Meer Mohr, J. C. (1935). Sur quelques malformations chez la limule, *Tachypleus gigas*. *Miscellanea Zoologica Sumatrana, 87*, 1–3.

Vendrasco, M. J., Kouchinsky, A. V., Porter, S. M., & Fernandez, C. Z. (2011). Phylogeny and escalation in *Mellopegma* and other Cambrian molluscs. *Palaeontologia Electronica, 14*, 1–44.

Vermeij, G. J. (1989). The origin of skeletons. *Palaios, 4*, 585–589.

Zacaï, A., Vannier, J., & Lerosey-Aubril, R. (2016). Reconstructing the diet of a 505-million-year-old arthropod: *Sidneyia inexpectans* from the Burgess Shale fauna. *Arthropod Structure & Development, 45*, 200–220.

Zelditch, M., Swiderski, D., Sheets, D. H., & Fink, W. (2004). *Geometric Morphometrics for Biologists: A primer*. Waltham, MA: Elsevier Academic Press.

Zhang, Z., & Brock, G. A. (2018). New evolutionary and ecological advances in deciphering the Cambrian explosion of animal life. *Journal of Paleontology*, *92*, 1–2.

Paper 1

Reappraising the early evidence of durophagy and drilling predation in the fossil record: implications for escalation and the Cambrian Explosion

Higher Degree Research Thesis by Publication

University of New England

STATEMENT OF ORIGINALITY

(To appear at the end of each thesis chapter submitted as an article/paper)

We, the Research Master/PhD candidate and the candidate's Principal Supervisor, certify that the following text, figures and diagrams are the candidate's original work.

Type of work	Page number/s
Scientific publication	13–43

Name of Candidate: Russell D. C. Bicknell

Name/title of Principal Supervisor: John R. Paterson

[redacted]

_____ 11/04/2019

Candidate Date

[redacted]

_____ 11/04/2019

Principal Supervisor Date

Higher Degree Research Thesis by Publication

University of New England

STATEMENT OF AUTHORS' CONTRIBUTION

(To appear at the end of each thesis chapter submitted as an article/paper)

We, the Research Master/PhD candidate and the candidate's Principal Supervisor, certify that all co-authors have consented to their work being included in the thesis and they have accepted the candidate's contribution as indicated in the *Statement of Originality*.

	Author's Name (please print clearly)	**% of contribution**
Candidate	Russell D. C. Bicknell	65
	John R. Paterson	35

Name of Candidate: Russell D. C. Bicknell

Name/title of Principal Supervisor: John R. Paterson

[redacted]

_____ 11/04/2019

Candidate Date

[redacted]

_____ 11/04/2019

Principal Supervisor Date

Paper 2

The gnathobasic spine microstructure of recent and Silurian chelicerates and the Cambrian artiopodan *Sidneyia*: Functional and evolutionary implications

Higher Degree Research Thesis by Publication
University of New England

STATEMENT OF ORIGINALITY

(To appear at the end of each thesis chapter submitted as an article/paper)

We, the Research Master/PhD candidate and the candidate's Principal Supervisor, certify that the following text, figures and diagrams are the candidate's original work.

Type of work	Page number/s
Scientific publication	49–61

Name of Candidate: Russell D. C. Bicknell

Name/title of Principal Supervisor: John R. Paterson

[redacted]

_____ 11/04/2019

Candidate Date

[redacted]

_____ 11/04/2019

Principal Supervisor Date

Higher Degree Research Thesis by Publication

University of New England

STATEMENT OF AUTHORS' CONTRIBUTION

(To appear at the end of each thesis chapter submitted as an article/paper)

We, the Research Master/PhD candidate and the candidate's Principal Supervisor, certify that all co-authors have consented to their work being included in the thesis and they have accepted the candidate's contribution as indicated in the *Statement of Originality*.

	Author's Name (please print clearly)	**% of contribution**
Candidate	Russell D. C. Bicknell	55
Other Authors	John R. Paterson	20
	Jean-Bernard Caron	10
	Christian B. Skovsted	15

Name of Candidate: Russell D. C. Bicknell

Name/title of Principal Supervisor: John R. Paterson

[redacted]

_____ 11/04/2019

Candidate Date

[redacted]

_____ 11/04/2019

Principal Supervisor Date

Paper 3

A 3D anatomical atlas of appendage musculature in the chelicerate arthropod *Limulus polyphemus*

PLOS ONE

RESEARCH ARTICLE

A 3D anatomical atlas of appendage musculature in the chelicerate arthropod *Limulus polyphemus*

Russell D. C. Bicknell[1]*, Ada J. Klinkhamer[2☯], Richard J. Flavel[3☯], Stephen Wroe[2‡], John R. Paterson[1‡]

1 Palaeoscience Research Centre, School of Environmental and Rural Science, University of New England, Armidale, Australia, **2** FEARLab, Palaeoscience Research Centre, School of Environmental and Rural Science, University of New England, Armidale, Australia, **3** Agronomy and Soil Science, School of Environmental and Rural Science, University of New England, Armidale, Australia

☯ These authors contributed equally to this work.
‡ These authors also contributed equally to this work.
* rdcbicknell@gmail.com

Citation: Bicknell RDC, Klinkhamer AJ, Flavel RJ, Wroe S, Paterson JR (2018) A 3D anatomical atlas of appendage musculature in the chelicerate arthropod *Limulus polyphemus*. PLoS ONE 13(2): e0191400. https://doi.org/10.1371/journal.pone.0191400

Editor: Yvan Rahbé, INRA, FRANCE

Received: March 21, 2017

Accepted: January 4, 2018

Published: February 14, 2018

Data Availability Statement: The 3D PDFs are supplementary files (S1–S8 Figs) that are available from the Dryad Digital Repository at the following DOI: 10.5061/dryad.vs044.

Funding: This research is supported by funding from an Australian Postgraduate Award (to RDCB) and an Australian Research Council Future Fellowship (FT120100770 to JRP). The funders had no role in study design, data collection and analysis, decision to publish, or preparation of the manuscript.

Abstract

Limulus polyphemus, an archetypal chelicerate taxon, has interested both biological and paleontological researchers due to its unique suite of anatomical features and as a useful modern analogue for fossil arthropod groups. To assist the study and documentation of this iconic taxon, we present a 3D atlas on the appendage musculature, with specific focus on the muscles of the cephalothoracic appendages. As *L. polyphemus* appendage musculature has been the focus of extensive study, depicting the muscles in 3D will facilitate a more complete understanding thereof for future researchers. A large museum specimen was CT scanned to illustrate the major exoskeletal features of *L. polyphemus*. Micro-CT scans of iodine-stained appendages from fresh, non-museum specimens were digitally dissected to interactively depict appendage sections and muscles. This study has revealed the presence of two new muscles: one within the pushing leg, located dorsally relative to all other patella muscles, and the other within the male pedipalp, located in the modified tibiotarsus. This atlas increases accessibility to important internal and external morphological features of *L. polyphemus* and reduces the need for destructive fresh tissue dissection of specimens. Scanning, digitally dissecting, and documenting taxa in 3D is a pivotal step towards creating permanent digital records of life on Earth.

Introduction

Advances in modern computed tomography (CT or serial x-ray), micro-computed tomography (micro-CT), synchrotron-radiation micro-CT and magnetic resonance imaging (MRI) technology have presented researchers interested in biological form and function the opportunity to study complex internal and external anatomical morphological features, without destroying specimens [1–3]. This technology was pivotal in driving the modern 'taxonomic

Competing interests: The authors have declared that no competing interests exist.

renaissance' and the understanding of external morphology and *in situ* internal features [1, 4]. The scans produced by these tools can be employed in 3D digital dissection and reconstruction of organisms in the form of interactive 3D PDFs [5, 6]. As anatomy is a three dimensional construct, 3D PDFs represent reality more accurately than 2D images in publications [7, 8]. Using interactive 3D models to illustrate organisms is a major step towards accurately documenting taxa and provides a platform for the easy and rapid dissemination of information [9].

The majority of research depicting organisms in 3D has considered vertebrates, while invertebrates were largely excluded from digital documentation until recently [7]. Invertebrate groups that have been documented in 3D include chelicerates [10–12], crabs [13], earth worms [2], gastropods [14–18] (to name a few), insects [19–23], monoplacophorans [24], polychaetes [25] and sea urchins [4]. Although not comprehensive, this list illustrates how few invertebrate groups have been digitally documented, compared to the number of known invertebrate clades. To expand this list, one of the archetypal chelicerates, *Limulus polyphemus* (Linnaeus), was selected for CT scanning, digital dissection and interactive three-dimensional PDF construction. The similarity of *L. polyphemus* to some extinct xiphosurans (such as the Jurassic *Mesolimulus walchi* (Desmarest)), coupled with the size and lifestyle of *L. polyphemus*, has made the taxon one of the most extensively studied arthropods from both biological and paleontological perspectives [26]. An extensive record of *L. polyphemus* muscles will allow studies that employ *L. polyphemus* as a modern analogue to present possible muscle combinations and place functional limits on motion and feeding ability for extinct taxa. Even though the internal and external features of *L. polyphemus* are regularly depicted as 2D illustrations in various publications, *L. polyphemus* has never been documented in 3D [27]. This study presents a three-dimensional interactive model of *L. polyphemus* appendages and muscles, along with a written description of the studied musculature.

Methods

Digital dissection was performed on one large (56-cm-long, including telson), dried, articulated female carcass of *Limulus polyphemus* (specimen number Va. 06) housed in the Natural History Museum of the University of New England (Armidale, New South Wales, Australia). It was scanned on a Siemens SOMATOM definition medical CT scanner at Armidale Radiology (Armidale, NSW, Australia). Scan data include 822 slices at a slice thickness of 0.75 mm. The scan was imported into Mimics 19.0 (Mimics 19.0, Materialise, Leuven, Belgium). A 3D model of the exoskeleton was created by segmenting the scan using the Mimics 'thresholding tool'. The main exoskeletal components of interest were modelled separately for closer inspection and description.

In addition to the complete specimen, fresh appendages of *Limulus polyphemus* were obtained from the Marine Biological Laboratory of Woods Hole, USA to document the appendages and associated muscles in greater detail. These specimens include articulated examples of one chelicera, one male pedipalp, one walking leg, one pushing leg, one set of chilaria, one genital operculum, and one gill operculum. Appendages were submerged in a solution of 1% iodine metal dissolved in pure ethanol for 13 days, following the procedure outlined in [28] and the staining time suggested in [29]. The walking leg was re-stained for another 13 days, as the first staining process failed to sufficiently highlight the muscles. After staining, specimens were washed thoroughly in ethanol and placed in ethanol for 2 days to leach any additional iodine before being scanned in the micro-CT (GE-Phoenix V|tome|xs micro CT scanner with 240kV 'Direct' tube) at the University of New England (UNE). Iodine staining of the appendages prior to CT scanning facilitates the observation of detailed muscle structures, without damaging the specimen (see [25, 28, 29]). Furthermore, as iodine staining

of arthropod specimens has previously identified microscopic features (e.g., single muscle fibers) [28], it is likely that all of the larger muscles have been discerned using this method. Micro-CT data of samples were captured using Datos acquisition software version 2.2.1 and reconstruction software version 2.2.1 RTM. The samples were mounted on the rotating stage and imaged using the previously determined optimal X-ray tube settings (150 kV, 200 μA, 200 ms integration time per projection, focal spot 4 μm diameter for the divergent, polychromatic source). Projections (3600 in 360 degrees) were captured using a 2000 x 1000 pixel 'virtual' (moving) detector array. The isotropic voxel side length varied with the sample size: 70.2 μm for the gill operculum, male appendage, walking and pushing legs, and set of chilaria and chelicera; 46.8 μm for the genital operculum. All scans were captured using the GE constant rotation CT function to improve acquisition time and sample movement during the scan.

The tomographs were imported into Mimics 19.0 to conduct a digital dissection, involving the segmentation of the exoskeleton and individual muscles in each appendage. Muscle descriptions were derived by studying the scans and 3D reconstructions, and identified using publications that previously detailed the muscles of interest [27, 30–35]. The muscles are numbered using Shultz's numbering system [27]—which was an expansion of Lankester's terminology [31]—to facilitate easy comparison between the reconstructions presented here and in Shultz's monumental work. However, in some cases, the muscles were previously ascribed names and so these have also been included in the descriptions. A total of 32 individual muscles were identified and described. Once the digital dissection was complete and muscles identified, 3D models of the exoskeleton and individual muscles were exported from Mimics and 3D PDFs were generated using 3D Reviewer [36]. 3D PDFs were created for each appendage as well as the overall specimen. Distinct muscles and exoskeletal elements were assigned different colours so they could be more easily differentiated from each other. For the 3D PDFs of the walking leg, pushing leg and male pedipalp, the exoskeletal components and muscles that are common across the PDFs are coloured the same. The same approach was applied to the genital operculum and gill operculum PDFs. As there are muscles common to the walking leg, pushing leg and male pedipalp, the most anatomically informative muscle reconstructions from these three PDFs were used to construct the in-text figures. The 3D PDFs are supplementary files (S1–S8 Figs) that are available from the Dryad Digital Repository at the following DOI: 10.5061/dryad.vs044.

Results

The results presented here provide a 3D atlas of the major external (exoskeletal) features of *L. polyphemus*, coupled with detailed images and descriptions of appendage musculature. During the construction of the atlas, two new muscles were identified: one from the male pedipalp and one within the pushing leg. Within the pushing leg, subdivisions for two muscles is presented. Interestingly, due to the additional (prolonged) staining of the walking leg, the muscles within this scan are shrunk in comparison to the pushing leg and male pedipalp. The interactive 3D models (S1–S8 Figs) should be considered in conjunction with the descriptions of the exoskeleton and muscles.

Dorsal shield

The dorsal shield of *Limulus polyphemus* consists of two major tagmata: the anterior cephalothorax, and the posterior thoracetron, both of which cover the more delicate ventral structures (Fig 1A and 1B) [26, 37–40]. The cephalothorax and thoracetron are connected by a soft arthrodial membrane hinge [38].

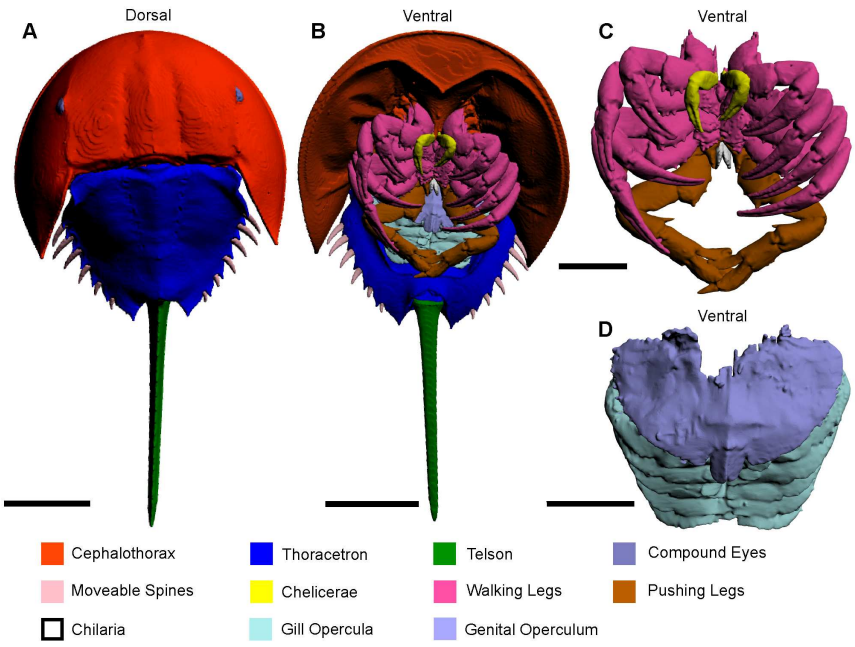

Fig 1. 3D reconstruction of the complete museum specimen (va.06) of *Limulus polyphemus* in dorsal and ventral aspect, as modelled from CT scanning. (A) Dorsal view of entire exoskeleton. (B) Ventral view of entire exoskeleton. (C) Detail of cephalothoracic appendages. (D) Detail of thoracetronic appendages. The interactive 3D version of this file is available in the Supporting Information (S1 Fig). Scale bars 100 mm for A, B; 50 mm for C, D.

https://doi.org/10.1371/journal.pone.0191400.g001

Cephalothorax

The anterior section is semicircular, margined by a lipped flange, with two lateral compound eyes and central ocelli (Fig 1A and 1B) [38, 41]. Three ridges are present on the cephalothorax: the median ridge that runs from the membranous hinge to the ocelli and bisects the dorsal shield, and two lateral ophthalmic ridges that are slightly convergent anteriorly and intercept the adaxial sides of the compound eyes [42]. Between each ophthalmic ridge and the median ridge is a longitudinal furrow [43]. On the underside of the cephalothorax are six pairs of prosomal appendages and one set of opisthosomal appendages [40].

Thoracetron

The hexagonal posterior section of the dorsal shield is bisected by a median ridge: a posterior continuation of the cephalothoracic median ridge (Fig 1A and 1B) [40, 42]. Flanking the median ridge are six pairs of entapophyseal pits: attachment sites for the six other opisthosomal appendages that are located on the underside of the thoracetron [40, 42]. Along the posterolateral margins of the thoracetron are six moveable spines housed within notches [40].

Telson

The most posterior component of the *Limulus polyphemus* exoskeleton is the telson. This triangular ridged spine attaches to the opisthosoma with a ball joint (Fig 1A and 1B). The ball joint attachment allows the telson to be highly moveable and permits righting of an overturned individual [26, 38, 44]. The telson is capable of rotating through a complete circle and has full 180˚ range of motion in the vertical plane [45, 46].

Appendages

Limulus polyphemus has 13 pairs of appendages (Fig 1B–1D). The first seven pairs of appendages are attached to the ventral side of the cephalothorax and are used for locomotion and feeding. The first six are segmented and the seventh is not. In order, starting from the anteriormost pair, there are the chelicerae (pair 1), walking legs (pairs 2–5), pushing legs (pair 6), and chilaria (pair 7). In males, the first pair of walking legs is modified during ontogeny into the so-called male pedipalp. There are six appendages attached to the ventral side of the thoracetron [39, 47]. The thoracetronic appendages are divided into two groups: the genital operculum (pair 8) and the five gill opercula that are used for respiration and swimming (pairs 9–13) [26, 39, 47].

Chelicerae

The chelicerae are a pair of forward facing appendages and consist of three segments: the protomerite, deutomerite and tritomerite (Fig 2A–2D) [31, 47]. The tritomerite is a moveable arm that functions with the fixed deutomerite to clasp, grip and manipulate food to the mouth after mastication by the waking and pushing legs [26, 27, 31, 39, 48]. There are four muscles within the protomerite, deutomerite and tritomerite [27].

Muscle 49—This muscle has an origin on the dorsolateral and ventroproximal section of the protomerite and an insertion on the dorsal margin of the deutomerite (Fig 2E and 2F) [27]. This elongate muscle is located ventrally relative to muscle 50.

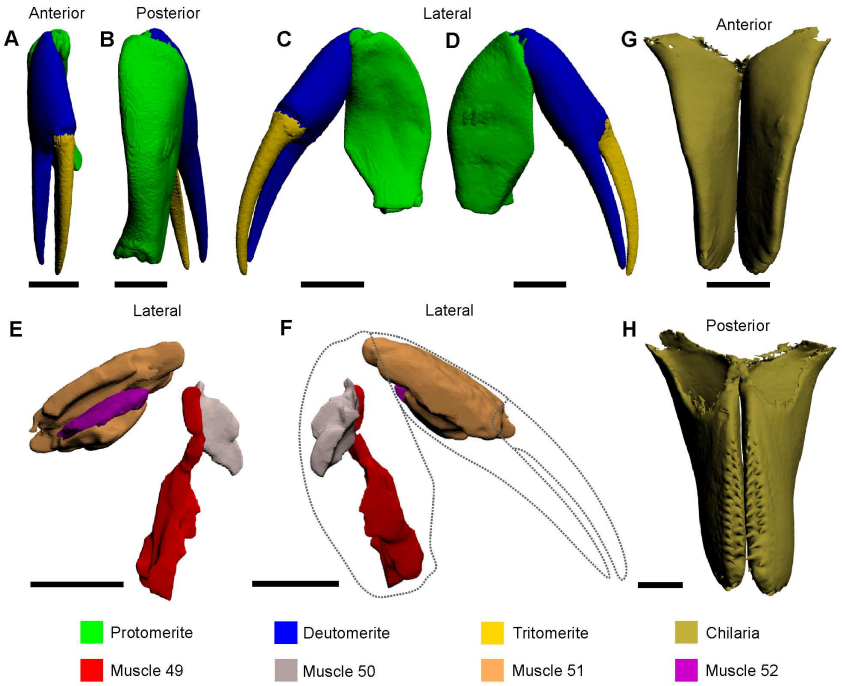

Fig 2. 3D reconstruction of a single chelicera (A–D) and muscles therein (E, F) and the chilaria (G, H), as modelled from iodine staining and micro-CT–scanning. The 3D versions of these files are available in the Supporting Information (S2 and S6 Figs). Dotted lines in F outline the protomerite, deutomerite and tritomerite to indicate the relative positions of the muscles. All scale bars 5 mm.

https://doi.org/10.1371/journal.pone.0191400.g002

Muscle 50—This muscle has an origin on the dorsomedial and ventroproximal section of the protomerite and an insertion on the ventral margin of the deutomerite (Fig 2E and 2F) [27]. This muscle is located dorsally relative to muscle 49.

Muscle 51—This muscle has three origins on the dorsal section of the deutomerite and an insertion on the medial margin of the tritomerite (Fig 2E and 2F) [27]. This muscle has three major components that are all elongate and located posteriorly relative to muscle 52.

Muscle 52—This muscle has an origin on the lateral section of the deutomerite and an insertion on the lateral margin of the tritomerite (Fig 2E) [27]. This muscle is very thin, elongate and located anteriorly relative to muscle 51.

Walking leg

There are four pairs of chelate walking legs [47] in the set of female appendages, and three pairs in the set of male appendages, as the first walking leg is modified into the male pedipalp during ontogeny (Fig 3A and 3B) [49]. Walking legs have six segments (proximally to distally):

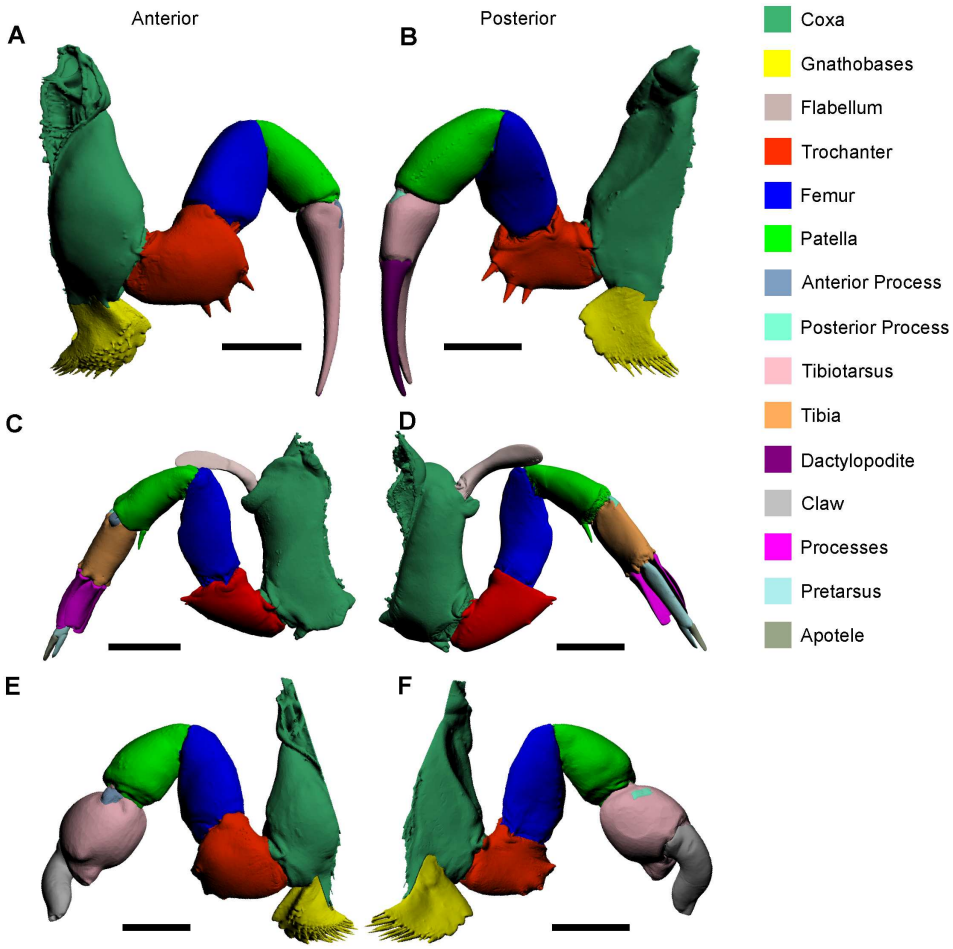

Fig 3. 3D reconstructions of the walking leg (A, B), pushing leg (C, D), and male pedipalp (E, F) as modelled from micro-CT scanning. Reconstructions in the left column (A, C, E) are all anterior views and reconstructions in the right column (B, D, F) are all posterior views. These reconstructions should be studied in conjunction with the muscle reconstructions in Fig 4. The 3D versions of these files are available in the Supporting Information (S3, S4 and S5 Figs). Scale bars 15 mm for A, B, E, F; 20 mm for C, D.

https://doi.org/10.1371/journal.pone.0191400.g003

the coxal endite that exhibits gnathobases; trochanter; patella; tibia; tibiotarsus; and the dactylopodite (referred to elsewhere as the claw or apotele) [26, 27, 31–34, 39, 49]. The dactylopodite is a moveable segment attached to the tibiotarsus, allowing these two segments to function together as claspers to move food to the gnathobases for mastication and shell breaking [49]. The main use of the walking legs is in locomotion and feeding, as they are radially arranged about the mouth [26, 39, 49–51]. There are 20 muscles in the walking legs (Fig 4A and 4B). Note that muscles 67–84 in the walking leg are the same as the male pedipalp, and muscles 67–82 in the walking leg are common to the pushing leg. The descriptions of the walking leg muscles 67–84 apply the male pedipalp, and the descriptions of walking leg muscles 67–82 apply to the pushing leg, so will not be redescribed in the pushing leg and male pedipalp sections.

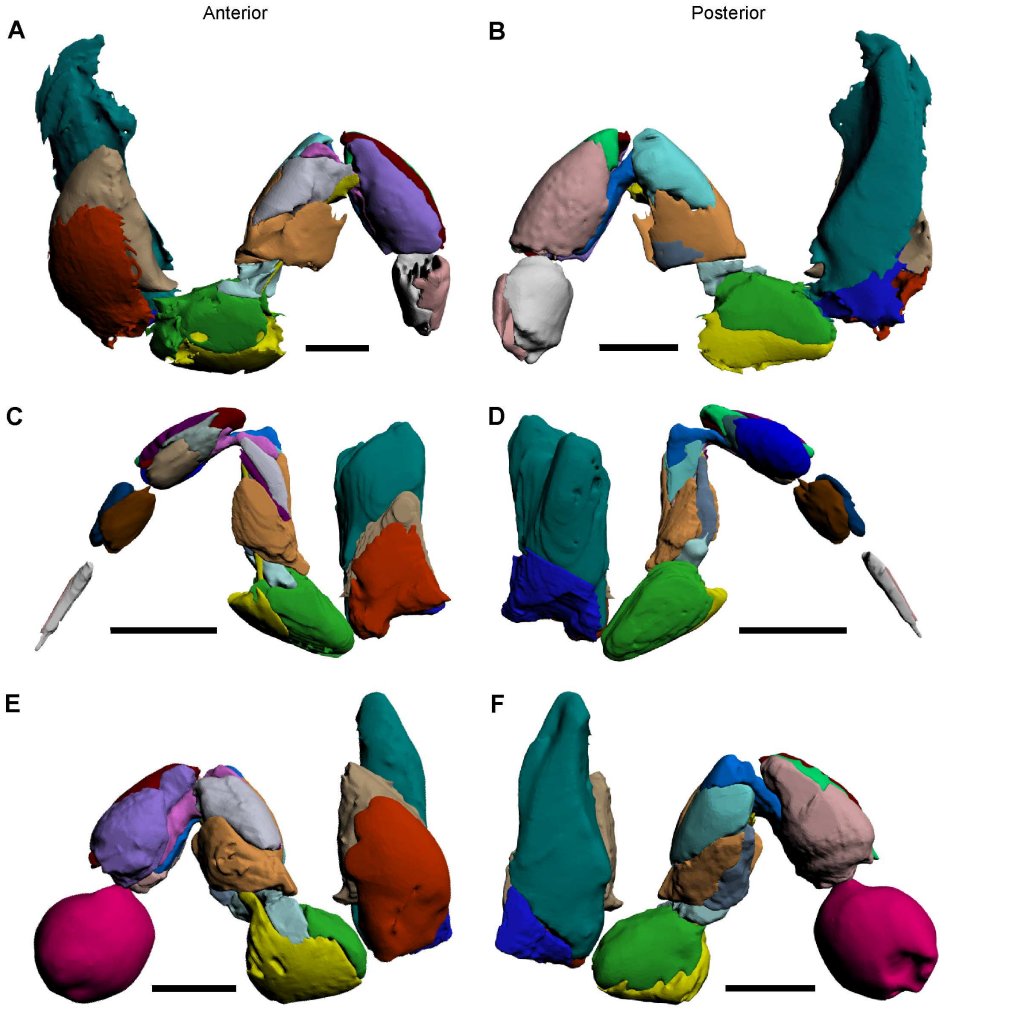

Fig 4. 3D reconstructions of identified muscles within the walking leg (A, B), pushing leg (C, D), and male pedipalp (E, F), as modelled from iodine staining and micro-CT–scanning. A key is not included, as deeper muscles cannot easily be visualized in this figure. Individual muscles of specific prosomal appendages are illustrated separately in Figs 5–8. Reconstructions in the left column (A, C, E) are all anterior views and reconstructions in the right column (B, D, F) are all posterior views. These reconstructions should be considered in conjunction with the cephalothoracic appendage reconstructions in Fig 3. The 3D versions of these files are available in the Supporting Information (S3, S4 and S5 Figs). Scale bars 10 mm for A, B, E, F; 20 mm for C, D.

https://doi.org/10.1371/journal.pone.0191400.g004

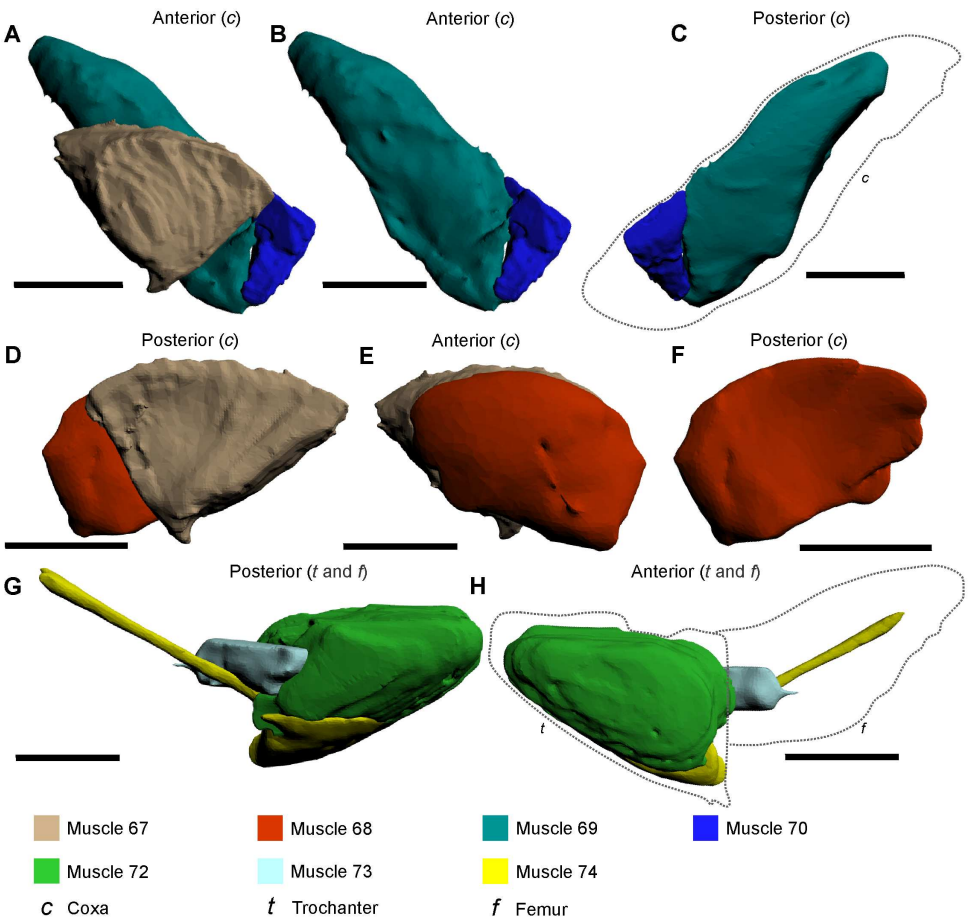

Fig 5. The muscles within the coxa, trochanter and femur of the walking legs, male pedipalp and pushing leg as modelled from iodine staining and micro-CT–scanning. The illustrated muscle reconstructions for A–F were selected from the male pedipalp 3D PDF (S4 Fig), and G–H were selected from the pushing leg PDF (S5 Fig), as these are considered to be the most anatomically informative. The muscles are depicted in anterior and posterior views to accurately display the main features and shapes, as well as positions relative to neighbouring muscles. The dotted line in C outlines the relative position of the coxal segment. The dotted lines in H outline the trochanter and femur. All scale bars 10 mm.

https://doi.org/10.1371/journal.pone.0191400.g005

Muscle 67—This muscle has an origin on the proximal anterior and posterior margins of the coxa and an insertion on the dorsal margin of the trochanter (Fig 5A, 5D and 5E) [27]. The muscle is located between muscles 68 and 69. This muscle has been named the *flexor trochanteris* [52] or the *trochanter levator* [30].

Muscle 68—This muscle has an origin on the ventral anterior section of the coxa and an insertion on the anteroventral margin of the trochanter (Fig 5D–5F) [27]. The muscle is located anteriorly relative to muscle 68. This muscle has been named the *trochanter depressor* [30], but is amended here as the *anterior trochanter depressor*.

Muscle 69—This muscle has an origin on the dorsal posterior and anterior sections of the coxa and an insertion on the ventral margin of the trochanter (Fig 5A–5C) [27]. The muscle is located between muscles 67 and 70. This muscle has been named the *flexor basis* [53] or the *trochanter depressor* [30], but is amended here as the *posterior trochanter depressor*.

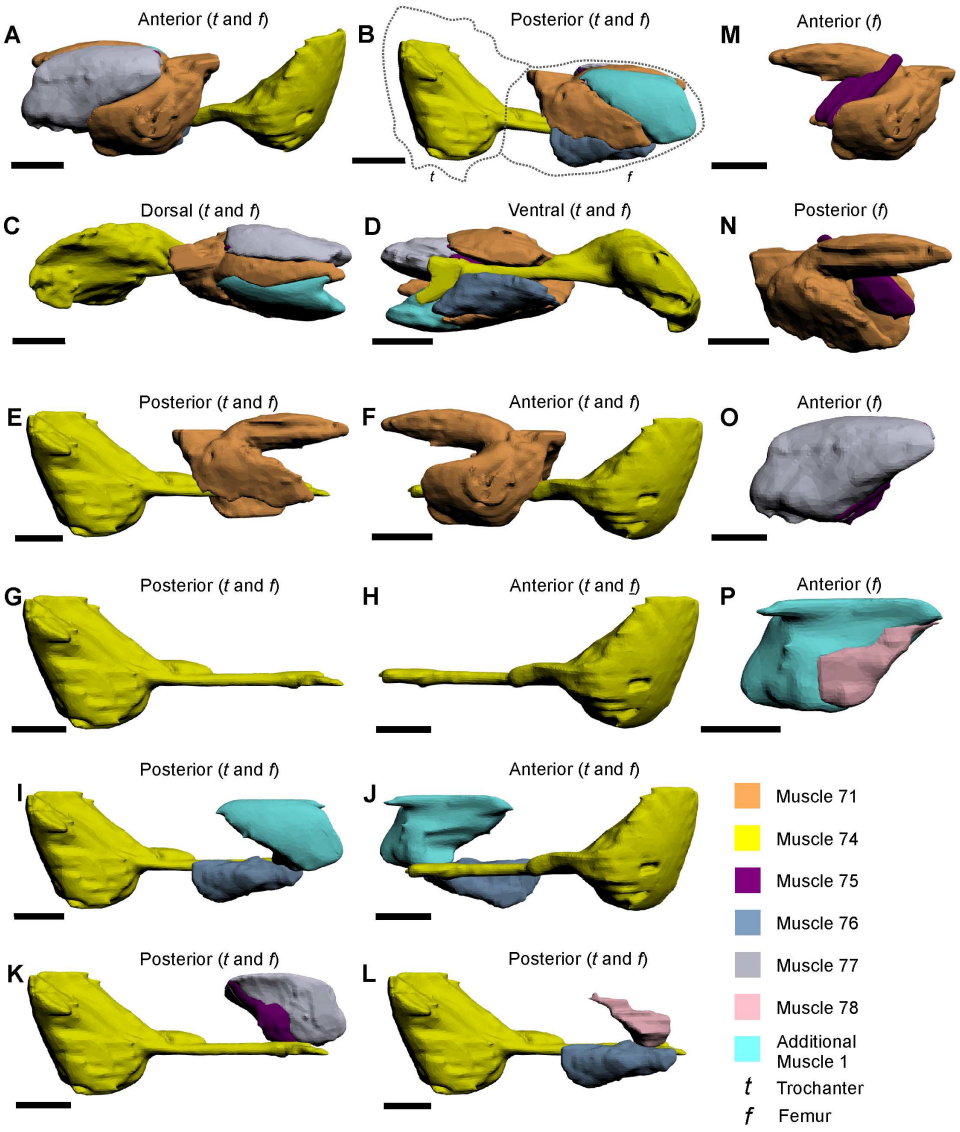

Fig 6. The muscles within the trochanter and femur of the walking legs, male pedipalp and pushing leg, as modelled from iodine staining and micro-CT–scanning. The illustrated muscle reconstructions were selected from the male pedipalp 3D PDF (S4 Fig), as these reconstructions are the most anatomically informative. A–D depict the seven femoral muscles and their relative positions to each other. The individual muscles (E–P) are shown in anterior and posterior views to accurately display the main features, shapes and, where possible, their position relative to adjacent muscles. The dotted lines in B outline the trochanter and femur. All scale bars 5 mm.

https://doi.org/10.1371/journal.pone.0191400.g006

Muscle 70—This muscle has the origin on the ventral posterior section of the coxa and an insertion on the posteroventral margin of the trochanter (Fig 5A–5C) [27]. The muscle is located posteriorly relative to muscle 69. This muscle has been named the *extensor basis maxillae* [53].

Muscle 71—This muscle has the origin on the dorsal section of trochanter-femur joint and insertions along the proximal anterior, posterior and dorsal sections of the femur (Fig 6A–6F, 6M and 6N) [27]. The muscle is narrow along the dorsal section of the femur and bifurcates into two lobes that flank the anterior and posterior sections of the femur. The muscle is located dorsally relative to muscles 73 and 74, posteriorly relative to muscles 75 and 77,

and anteriorly relative to 'Additional Muscle 1' and muscle 78. This muscle has been named the *femur levator* [30], *flexor merioni enemiique* [53] or the *ischiopodite extensor* [54].

Muscle 72—This muscle has an origin on the posterior and ventroposterior sections of the trochanter and an insertion on the posterior ventral margin of the femur (Fig 5G and 5H) [27]. The muscle is located dorsally relative to muscle 74 and proximally relative to muscle 73. This muscle has been named the *femur depressor* [30] or the *ischiopodite flexor* [54].

Muscle 73—This muscle has an origin on the distal anterior section of the trochanter and an insertion on the proximal posterior section of the femur (Fig 5G and 5H) [27]. This muscle is located distally relative to muscle 72. Fourtner & Sherman [54] suggested that this muscle was part of muscle 72 and was referred to as the *ischiopodite flexor*. As muscles 72 and 73 are distinct muscles, this name must be changed, but it is worth noting that the muscle functions as a flexor.

Muscle 74—This muscle has an origin on the anterior and ventral sections of the trochanter and has an insertion on the proximal end of the patellar sclerite (modelled together as one object) (Figs 5G, 5H and 6A–6L) [27, 47]. This muscle attaches to the so-called patellar sclerite, a tendon that that runs the length of the femur [27, 33, 47]. As muscle 74 and the patellar sclerite are grouped together here, muscle 74 is located ventrally relative to muscles 71, 76–80 and 'Additional Muscle 1'. This muscle has been named the *flexor femoris* [32], *femoro-patella flexor* [30], *merional entapophysis* [53], *mero-carpopodite flexor* [54] or Pringle's '*special muscle*' [52].

Muscle 75—This muscle has an origin on the middle dorsoanterior section of the femur and an insertion on the distal section of the patellar sclerite of muscle 74 (Fig 6D, 6K, 6M and 6N) [27]. This muscle is very thin, elongate, and is located posteriorly relative to muscle 77 and anteriorly relative to the patellar sclerite. Due to the thin nature of muscle 75, this muscle could not be reliably identified in the micro-CT scan of the walking leg, but is illustrated in the pushing leg and the male pedipalp PDFs. Due to the difficulty in identifying this muscle, it is possible that muscle 75 may be a part of the larger muscle 77.

Muscle 76—This muscle has an origin on the middle ventroposterior section of the femur and has an insertion on the distal shaft of the patellar sclerite (Fig 6B, 6D, 6I, 6J and 6L) [27]. This muscle is located posteriorly relative to the distal half of the patellar sclerite. The muscle has been previously grouped with muscle 74, 77 and 'Additional Muscle 1', and called the *mero-carpopodite flexor* [54]. As muscle 76 is a distinct muscle, the name is redundant.

Muscle 77—This muscle has an origin on the distal anterior section of the femur with an insertion on the distal anterior side of the patellar sclerite (Fig 6C, 6D, 6F and 6O) [27]. The muscle runs parallel to the distal anterior margin of the femur. This muscle has been called *femoro-patella flexor* [30], but is amended here to *anterior femoro-patella flexor*. Muscle 77 has been grouped with muscle 74, 76 and 'Additional Muscle 1', and called the *mero-carpopodite flexor* [54]. As muscle 77 is a distinct muscle, the name is redundant.

Additional Muscle 1—This muscle has an origin on the distal posterior section of the femur with an insertion on the distal posterior section of patella sclerite (Fig 6B–6D, 6I, 6J and 6P). The muscle is parallel to the distal posterior margin of the femur and located posteriorly relative to muscle 78. This muscle was not illustrated or noted in Shultz's review, but has been mentioned previously [30, 54]. This muscle has been called the *femoro-patella flexor* [30], but is amended here to *posterior femoro-patella flexor*. 'Additional Muscle 1' has

previously been grouped with muscle 74, 76 and 77, and called the *mero-carpopodite flexor* [54]. As 'Additional Muscle 1' is a distinct muscle, the name *mero-carpopodite flexor* is redundant.

Muscle 78—This muscle has an origin on the distal posterior section of the femur and has an insertion on the distal posterior section of the patellar sclerite (Fig 6L and 6P) [27]. This muscle is very thin and runs the distal length of the posterior side of the patellar sclerite. Due to the thin nature of muscle 78, this muscle was not reliably identified in the walking leg scan, but is illustrated in the pushing leg and the male pedipalp 3D PDFs. Due to the difficulty in identifying the muscle, muscle 77 may be a part of the larger 'Additional Muscle 1'.

Muscle 79—This muscle has origins on the distal part of the dorsal section of the femur and the anterior and anteroventral sections of the patella, with an insertion on the ventral margin of the tibiotarsus in the walking legs and male pedipalp, and the tibia in pushing legs (Fig 7A–7E, 7K, 7M and 7O) [27]. This muscle is elongate and is located posteriorly relative to muscle 81 and runs parallel with muscle 80. This muscle has been called the *propodite flexor* [54], and the *large leg muscle* [52], but is amened here as the *anterior propodite flexor*.

Muscle 80—This muscle has an origin on the distal part of the dorsal section of the femur, and the posterior and posteroventral sections of the patella, with an insertion on the ventral margin of the tibiotarsus in the walking legs and male pedipalp, and the tibia in the pushing legs (Fig 7A–7E, 7G and 7K) [27]. This muscle is slender and is located posteriorly relative to muscle 82 and runs parallel with muscle 79. This muscle has been called the *propodite flexor* [54], but is amended here as the *posterior propodite flexor*.

Muscle 81—This muscle has an origin on the anterodorsal section of the patella and an insertion on the anterior process of the tibiotarsus (Fig 7A–7C, 7E–7G, 7I, 7K, 7L and 7N) [27]. The muscle tapers rapidly into an elongated strip that runs through to the anterior process and is located anteriorly relative to muscle 79 and posteriorly relative to muscle 83. This muscle has been called the *propodite extensor* [52], but is amended here as the *anterior propodite extensor*.

Muscle 82—This muscle has an origin on the posterodorsal section of the patella and an insertion on the posterior process of the tibiotarsus (Fig 7B, 7C, 7H, 7K, 7M and 7N) [27]. The muscle tapers rapidly into an elongated strip that runs through to the posterior process. The muscle is located anteriorly relative to muscle 84, posteriorly relative to muscle 80, and runs parallel with muscle 81. This muscle has been called the *propodite extensor* [52], but is amended here as the *posterior propodite extensor*.

Muscle 83—This muscle has an origin on the anterior section of the patella and an insertion on the anterior margin of the tibia (Fig 7A, 7C, 7D, 7F and 7K–7O) [27]. This muscle is located anteriorly relative to muscle 81. This muscle has been named the *anterior patella-tibial flexor* [30]. Fourtner & Sherman thought that muscle 83 was divided into two muscles: the *anterior propodite flexor* and *anterior propodite extensor* [54]. As muscle 83 is clearly one muscle (at least within the walking leg and male pedipalp), both names, the *anterior propodite flexor* and *anterior propodite extensor*, should not be used.

Muscle 84—This muscle has an origin on the posterior section of the patella and an insertion on the posterior proximal margin of the tibiotarsus (Fig 7B–7E and 7G–7J) [27]. This muscle is located posteriorly relative to muscle 82. This muscle has been named the *posterior*

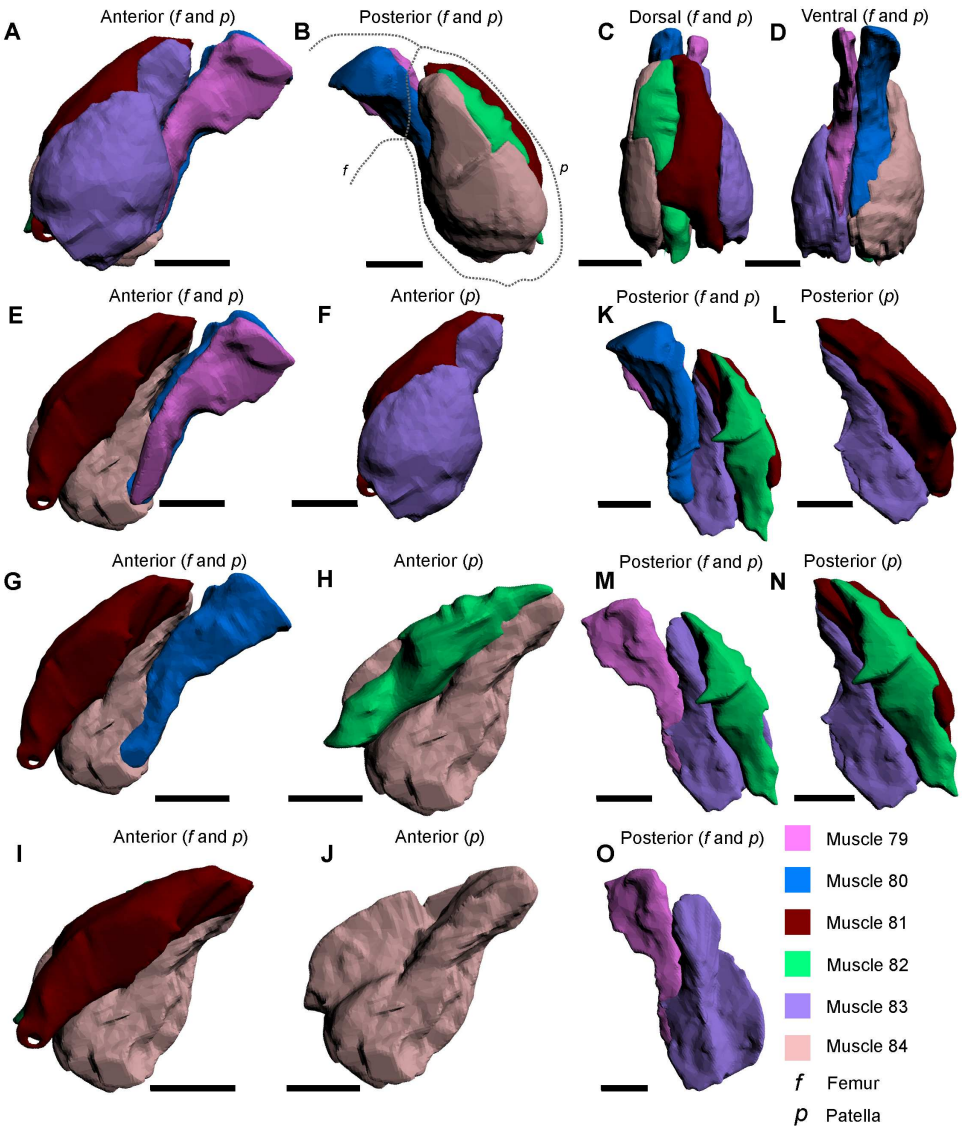

Fig 7. The muscles within the walking legs and male pedipalp patella, as modelled from iodine staining and micro-CT–scanning. The illustrated muscle reconstructions were selected from the male pedipalp 3D PDF (S4 Fig), as these reconstructions are the most anatomically informative. A–D depict the six muscles in four views to illustrate the overall form of the muscles and their relative positions to each other. The muscles (E–O) are shown in anterior and posterior views to accurately display the main features and shapes thereof and, where possible, their position relative to adjacent muscles. The dotted lines in B outline the distal end of the femur and the patella. All scale bars 5 mm.HHh.

https://doi.org/10.1371/journal.pone.0191400.g007

patella-tibial flexor [30]. Fourtner & Sherman thought that muscle 84 was divided into two muscles: the *posterior propodite flexor* and *posterior propodite extensor* [54]. As muscle 84 is clearly one muscle (at least within the walking leg and male pedipalp), both names, the *posterior propodite flexor* and *posterior propodite extensor*, should not be used.

Muscle 87—This muscle has an origin on the dorsal section of the tibiotarsus and an insertion on the dorsal margin on the dactylopodite (Fig 8N and 8P) [27]. Muscle 87 is located dorsally relative to muscle 88 and has been named the *abductor dactylis* [32] and the *claw opener* [52]. Fourtner & Sherman split this muscle into the *dactylopodite flexor* and *dactylopodite extensor* [54]. As muscle 87 is clearly one muscle, and the divisions presented in [54]

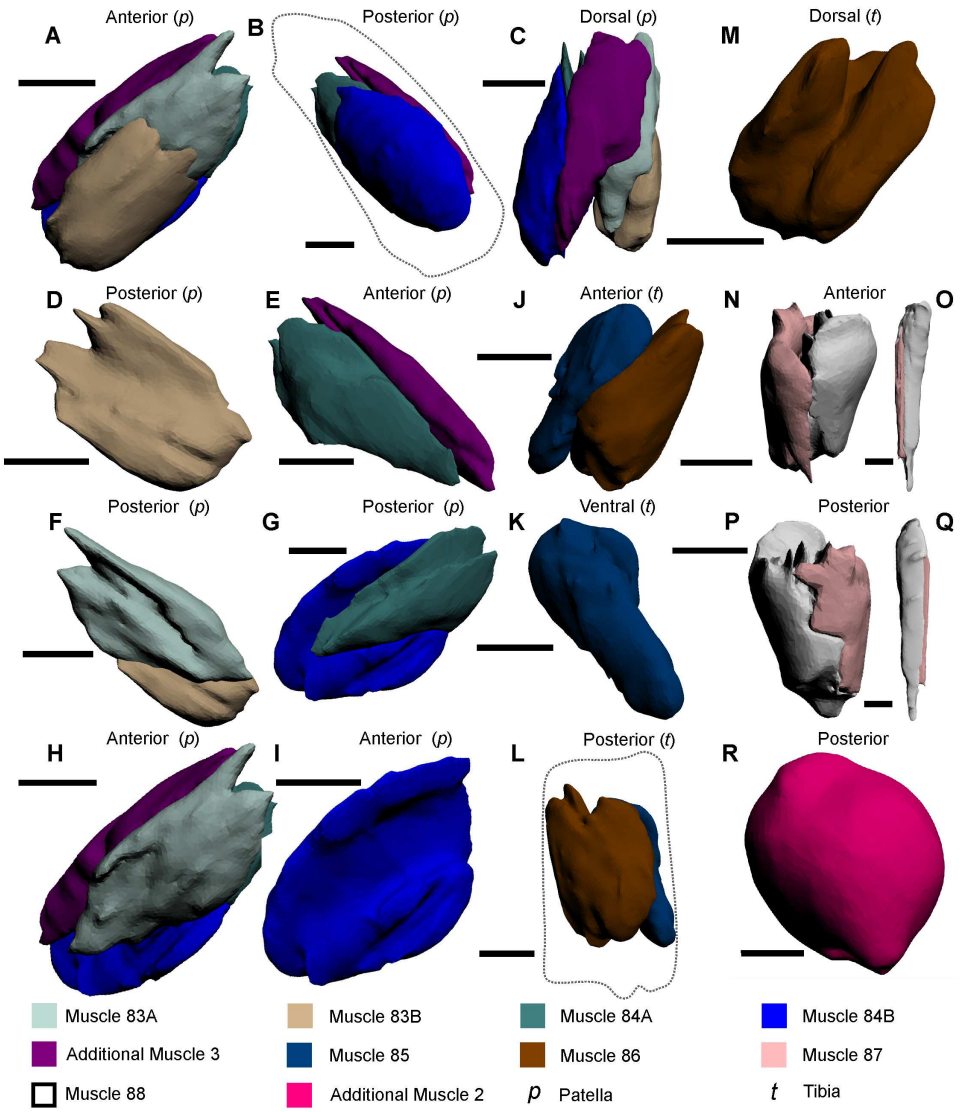

Fig 8. The muscles within the patella, tibia and pretarsus of the pushing leg, and the walking leg and male pedipalp tibiotarsus muscles, as modelled from iodine staining and micro-CT–scanning. (A–C) The five muscles within the patella of the pushing leg in three views to illustrate the overall form of the muscles. (D–I) Each of the five muscles in anterior and posterior views to accurately display the main features and shapes thereof and, where possible, their position relative to adjacent muscles. (J–M) The two muscles within the tibia of the pushing leg. (N, P) The two muscles within the tibiotarsus of the walking leg. (O, Q) The two muscles within the pretarsus of the pushing leg. (R) The newly described muscle within the tibiotarsus of the male pedipalp; due to the subspherical nature thereof, the anterior perspective was not included. Muscle reconstructions A–M, O and P were selected from the pushing leg 3D PDF (S5 Fig). The muscle reconstructions of N and P were selected from the walking leg 3D PDF (S3 Fig). The muscle reconstruction of R was selected from the male pedipalp (S4 Fig). The dotted line in B outlines the pushing leg patella. The dotted line in L outlines the tibia. Scale bars 5 mm for A–N, R; 4 mm for P; 3 mm for O, Q.

https://doi.org/10.1371/journal.pone.0191400.g008

do not reflect what was identified in the micro-CT scans, the names *dactylopodite flexor* and *dactylopodite extensor* should not be used.

Muscle 88—This muscle has an origin on the ventral section of the tibiotarsus and an insertion on the ventral margin of the dactylopodite (Fig 8N and 8P) [27]. This muscle is located

ventrally relative to muscle 87. Fourtner & Sherman split this muscle into the *dactylopodite flexor* and *dactylopodite extensor* [54]. As muscle 88 is clearly a single muscle, and the divisions presented in [54] do not reflect what was identified in the micro-CT scans, the names *dactylopodite flexor* and *dactylopodite extensor* should not be used.

Male pedipalp

The male pedipalp is effectively a modification on the anteriormost pair of walking legs (Figs 3E, 3F, 4E and 4F). While the coxa, trochanter, patella and tibia are the same, the tibiotarsus and dactylopodite are modified during ontogeny into a fortified bulbous section (the tibiotarsus) and a thick, curved claw (the dactylopodite) for mating purposes [26, 31]. The claw is often lost during the first mate pairing and is therefore not often observed [42]. Muscles 67–84 in male pedipalps are the same as those in the walking legs, so are not described again here. However, the muscles within the tibiotarsus are different in these appendages. In the bulbous tibiotarsus of the male pedipalp, a mass of dense muscle (called 'Additional Muscle 2') is present, whereas the walking leg tibiotarsus possesses muscles 87 and 88. The muscle mass within the trochanter has, to the knowledge of the authors, never been previously documented.

'Additional Muscle 2'—This muscle has an origin on the proximal margin of the tibiotarsus and an insertion on the dorsal margin of the tibiotarsus (Fig 8R). The muscle is not immediately adjacent to any other muscles, but is distal to the muscles within the patella. Here it is hypothesized that 'Additional Muscle 2' is modified during ontogeny into a single muscle mass to reflect the different use of the appendage and fortify the tibiotarsus and claw for grabbing during mating.

Pushing leg

The largest of the cephalothoracic appendages is the pushing leg, the main function of which is to push the animal forward, but also to assist in burrowing with the aid of the processes (Fig 3C and 3D) [26, 30]. The pushing leg has nine segments (proximally to distally): the coxal endite that bears a spatulate flabellum (also termed the epipodite [55]) and thick gnathobases; trochanter; femur; patella; tibia; an elongated pretarsus partially surrounded by four processes; and a moveable apotele [26, 27, 31, 47, 53]. Muscles 67–82 in the pushing legs are the same as those found in the walking legs and male pedipalp, so are not described again here. However, muscles 85, 86 and 'Additional Muscle 3' are unique to the pushing leg and so are described here. Furthermore, subdivisions of muscles 83 and 84 are presented. Finally, as muscles 87 and 88 in the pushing leg are located within the pretarsus, these muscles are re-described.

Muscle 83A—This subdivision of muscle 83 has an origin on the anterior section of the patella and an insertion on the distal margin of muscle 81 (Fig 8A, 8C, 8F and 8H). This muscle is located anteriorly relative to muscles 80, 81, and 84A. As muscle 83 has been named the *anterior patella-tibial flexor* [30], it is suggested that only 83A be called the *anterior patella-tibial flexor* and 83B be given a different name (see below).

Muscle 83B—This subdivision of muscle 83 has an origin on the centroanterior section of the patella and an insertion on the anterior margin on the tibia (Fig 8A, 8C, 8D and 8F). Muscle 83B is located anteriorly relative to muscle 83A. As muscle 83 has been named the *anterior patella-tibial flexor* [30] (discussed above), it is suggested here that 83B should be named the *anteriormost patella-tibial flexor*.

Muscle 84A—This subdivision of muscle 84 has an origin on the posterior section of the patella and an insertion on the distal margin of muscle 80 (Fig 8A–8C, 8E and 8G). This muscle is located posteriorly relative to muscles 80, 81 and 83A. As muscle 84 has been named the *posterior patella-tibial flexor* [30], it is suggested that only 84A be called the *posterior patella-tibial flexor* and 84B be given a different name (see below).

Muscle 84B—This subdivision of muscle 84 has an origin on the centroposterior section of the patella insertion on the posterior proximal margin of the tibia (Fig 8A–8C and 8G–8I). This muscle is located posteriorly relative to muscle 84A. As muscle 84 has been named the *posterior patella-tibial flexor* [30] (discussed above), it is suggested here that 84B be named the *posteriormost patella-tibial flexor*.

Additional Muscle 3—This muscle has not previously been described and does not resemble any other muscles described here (Fig 8A–8C, 8E and 8H) [27, 33, 47]. The muscle has an origin on the proximal dorsal section of the patella and an insertion on the dorsal margin of the tibia. This muscle is located dorsally relative to muscles 79–84A. Fourtner & Sherman [54] included a possible depiction of this muscle, but did not describe the muscle.

Muscle 85—This muscle has an origin on the anterior section of the tibia and has an insertion on the anterior margin of the pretarsus (Fig 8J–8L) [27]. This muscle is located dorsally relative to muscle 86.

Muscle 86—This muscle has an origin on the anterior and posterior sections of the tibia and an insertion on the posterior margin of the pretarsus (Fig 8J, 8L and 8M) [27]. This muscle bifurcates along the ventral margin of the tibia and is located ventrally relative to muscle 85.

Muscle 87—This muscle has an origin on the dorsal section of the pretarsus and an insertion on the dorsal margin of the apotele (Fig 8O and 8Q). This muscle is elongate, very thin and located dorsally relative to muscle 88. This muscle has been named the *abductor dactylis* [32].

Muscle 88—This muscle has an origin on the ventral section of the pretarsus and an insertion on the ventral margin of the apotele (Fig 8O and 8Q). This muscle is elongate, but thicker than the co-occurring muscle 87 and located ventrally relative to muscle 87.

Chilaria

These small, spine-bearing appendages are the most posterior, heavily modified and unsegmented cephalothoracic appendages that are also considered to be the first of the opisthosomal appendages (Fig 2G and 2H) [40, 47]. The chilaria have no internal musculature and function mostly as a means of preventing food items escaping behind the pushing legs [47].

Genital operculum

This opisthosomal appendage is located anteriorly to the gill opercula and attaches to the membrane that connects the cephalothorax and thoracetron (Fig 9A–9C) [47]. The genital operculum covers and protects the other thoracetronic appendages, as well as bearing the sexual organs [42]. The genital operculum consists of two plates, divided by the sternal lobe [27, 31, 39, 42]. Attached to each plate is an exopodial lobe, onto which an endopodite attaches [27, 31, 39, 42]. Additional features include the two genital papillae, the muscle masses that attach the genital operculum to the thoracetron, and the soft tissue that connects the genital operculum to the anteriormost gill operculum. Of the 16 muscles in the genital operculum, only the

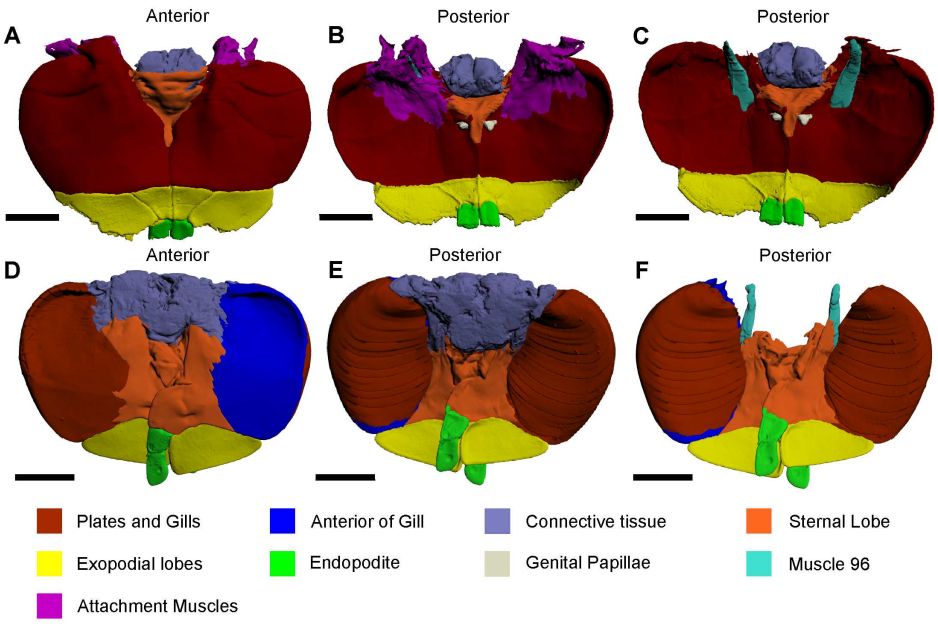

Fig 9. Anterior and posterior views of thoracetronic appendages, as modelled from iodine staining and micro-CT scanning. (A, B) Anterior and posterior views of the genital operculum. (D, E) Anterior and posterior views of a gill operculum. (C, F) Posterior views of the genital operculum and the gill operculum, respectively, with sections removed to depict muscle 96. The reconstructions in A–C were selected from the genital operculum 3D PDF (S7 Fig). The reconstructions in D–F were selected from the gill operculum 3D PDF (S8 Fig). All scale bars 20 mm.HHh.

https://doi.org/10.1371/journal.pone.0191400.g009

largest muscle is described and illustrated here, as this was the only muscle that could be definitively identified from the micro-CT scans [27, 47].

Muscle 96 on the genital operculum—This muscle has an origin on the posterior section of the cephalothorax and an insertion on the anterior margin of the genital operculum (Fig 9C) [27]. The muscle is elongate and is located adjacent to the thinner muscle 100, which was not reliably identified in the micro-CT scan and was therefore not figured. This muscle is called the *promotor muscle* [45, 47].

Gill operculum

The five most posterior appendage pairs of the exoskeleton are the gill (or branchial) opercula that attach to the ventral side of the thoracetron (Fig 9D–9F) [38, 40]. The gill opercula are used for respiration and osmoregulation, and also act as paddles to assist propulsion during swimming [26, 38, 56]. Each pair of gills consists of closely spaced brachial lamellae, of which there are at least 80 in adult individuals [47]. The gill pairs attach to plates that are divided by a sternal lobe [31]. Each plate attaches to an exopodial lobe, while two endopodites attach to the distal sections of the sternal lobe [26, 27, 31, 38, 39, 56]. An additional feature includes the connective tissue that attaches the gill opercula to the thoracetron, but also join the set of thoracetronic appendages [27]. The largest of 16 muscles in each gill operculum is described and illustrated here, as this was the only muscle that could be definitively identified in the micro-CT scans [27, 47].

Muscle 96 on the gill opercula—This muscle has an origin on the thoracetron, at the entapophyseal pits, and an insertion on the anterior margin of the gill opercula (Fig 9F) [27]. The

muscle is elongate and located adjacent to the thinner muscle 100, which was not reliably identified in the micro-CT scan and was therefore not figured. This muscle is called the *promotor muscle* [47].

Discussion

Muscles in 3D

Studying the muscles of *Limulus polyphemus* using a 3D approach allows researchers interested in chelicerate appendage musculature to consider such anatomy in a biologically accurate manner. The segmentation of muscles identified two new muscles that are described here. This result illustrates how useful *in vivo* muscle studies after iodine staining can be: even with the most careful dissection, muscles can be missed or lumped together unintentionally. Furthermore, digital dissections can be conducted multiple times and one is not constrained by the possibility of the muscles decaying, like standard dissections. The 3D PDFs constructing this atlas offer a resource for researchers interested in visualizing *L. polyphemus* muscles, but also general external morphology, in a manner that reflects the three dimensional nature of the organism. Beyond this general interest, there are other important applications of this study. As *L. polyphemus* is employed as an outgroup for arachnid phylogenies that include both external exoskeleton and muscle characters [33], 3D reconstructions can aid in more accurate coding. Furthermore, as *L. polyphemus* is used as a modern analogue for suggesting the mode of life for extinct taxa, such as the Cambrian arthropod *Sidneyia inexpectans* (Walcott) from the Burgess Shale of Canada [57], and the Silurian eurypterid *Eurypterus tetragonophthalmus* Fischer from Estonia [58], appendage muscle data are useful. An accurate record of *L. polyphemus* muscles can help researchers to suggest possible muscle combinations and arrangements within extinct taxa and, by extension, place functional limits on appendage motion and feeding ability.

Iodine staining

Iodine staining of the appendages to highlight muscles within the exoskeletal segments was an excellent method for studying these anatomical structures in detail. A standard micro-CT scan cannot easily differentiate soft tissue unless the tissue has differing x-ray attenuation properties compared to the surrounding material [59]. As non-biomineralized material has low X-ray absorption and contrast, the addition of iodine solution to the tissue results in the ability to observe soft tissue features in much greater detail [28, 29]. Although the micro-CT scanner would have identified the exoskeleton regardless, the utilization of iodine staining facilitated the clear differentiation of muscles that would not have been possible with unstained specimens. Metscher [28] illustrated this same result with insects, but the present study is the first to extend iodine staining to chelicerates. As a topic of further investigation, it would be interesting to compare the results of micro-CT scans of stained arthropod appendages (or complete specimens) to those that have combined both micro-CT and MRI scans of non-stained specimens.

Studying the scans of iodine-stained specimens in conjunction with anatomical drawings demonstrates that researchers need not conduct physical dissections to identify muscles. This is advantageous in the study of arthropod anatomy, as removing the exoskeleton to identify and examine muscles is a complicated task that often precludes the consideration of their 3D structure. However, care must be taken, as extended periods of staining using this method will dehydrate specimens severely and affect the identification of muscles. This is depicted here in

the reconstructions of the walking leg: the muscles within this scan are shrunk in comparison to the pushing leg and male pedipalp (S3–S5 Figs). It is therefore imperative that when conducting iodine staining using the method outlined here, that the specimens not be housed in alcohol for extensive periods. Expanding on the present study using iodine staining to include detailed investigation of other anatomical components of *L. polyphemus* may reveal additional, as-yet undocumented internal anatomy of *L. polyphemus*. While a study of this magnitude was beyond the scope of this work, the information derived from subsequent studies would be of particular value in arthropod taxonomy and phylogeny, as internal anatomy is often important for the classification of various groups [7].

Digital specimens

Biological collections housed in various institutions, especially museums, have academic, cultural and historic value, so it is important that specimens be made available (in one way or another) to researchers interested in studying them, but also the public at large. One way is to provide photos and other forms of illustration (e.g., line drawings) in publications, on websites, and other forms of media. However, conventional 2D illustrations of museum specimens can be somewhat limited in the anatomical information they provide. To gain a better understanding of the 3D nature of specimens, it is often necessary for researchers to visit institutional collections or borrow the material in order to physically examine them, which in either case can be impractical for various reasons relating to rarity, fragility, logistics, cost, or policy. Ideally, morphologically unique or interesting museum specimens, not to mention important type material, should be scanned using an MRI, CT or micro-CT scanner for the purpose of re-descriptions, digital dissections, and the production of morphological datasets. Using such an approach, researchers will have access to fundamental, historical and revised taxonomic data. These datasets remove the need for taxonomic housekeeping—the reconsideration of archaic taxon descriptions and fruitless efforts to locate specimens that sometimes no longer exist [60–62]. This is not to suggest that digital records should replace physical specimens, but simply provide researchers with another medium through which organisms can be studied. To see this suggestion become reality, museums and other collection-focused research institutions need to take the lead in compiling the digital collections of useful specimens [25, 28]. This study is an example of how this can be done: an informative museum specimen of *Limulus polyphemus* was used to construct an atlas and re-describe various anatomical features of this important taxon [61].

Nomenclature

As this atlas re-describes various anatomical parts of *Limulus polyphemus*, a short comment on the general lack of consistency in terminology within the existing literature is warranted. In reviewing the terms assigned to the external exoskeletal features of *L. polyphemus*, it became apparent that multiple names for various components of the exoskeleton have been employed, resulting in confusion. Thus, there is a need to standardize the terminology. It is suggested that the names for exoskeletal components assigned in the 3D PDFs be adopted henceforth. The names suggested will hopefully remove any confusion regarding the terminology of the cephalothoracic appendages, especially the most distal segments. Conversely, after considering the wealth of literature on this extensively studied taxon, there are 11 muscles within the cephalothoracic appendages alone that are described, but remain un-named. Therefore, an opportunity exists for arthropod experts to suggest names for these muscles and preclude the need for a numerical system. Assigning names to muscles is especially important as the numbering system has been employed for *L. polyphemus* since Lankester (1881) [31].

Conclusion

Limulus polyphemus is described and digitally dissected for the first time in 3D. A CT scan of a large museum specimen depicts the main exoskeletal features, while micro-CT scans of fresh, iodine-stained appendages have facilitated the digitization of appendage segments and muscles. A redescription of the appendage musculature is provided, including the identification of two new muscles, one in the pushing leg ('Additional Muscle 3') and one in the male pedipalp ('Additional Muscle 2'). In addition, two muscles within the pushing leg (muscles 83 and 84) are further subdivided: muscles 83A, 83B, 84A and 84B. This atlas represents the most biologically accurate 3D representation of *L. polyphemus* to date, and with a focus on the appendages and their associated muscles, makes the dataset an invaluable resource for researchers interested in the detailed anatomy of this iconic arthropod. The production of 3D atlases for other iconic and rare taxa will create important digital records that will improve accessibility to anatomical information and supplements the physical examination of specimens for taxonomic or other studies.

Supporting information

S1 Fig. 3D interactive model of the complete *Limulus polyphemus* specimen, as modelled from CT-scanning.
(PDF)

S2 Fig. 3D interactive model of the *Limulus polyphemus* chelicera, as modelled from iodine staining and micro-CT-scanning.
(PDF)

S3 Fig. 3D interactive model of the *Limulus polyphemus* walking leg, as modelled from iodine staining and micro-CT-scanning.
(PDF)

S4 Fig. 3D interactive model of the *Limulus polyphemus* male pedipalp, as modelled from iodine staining and micro-CT-scanning.
(PDF)

S5 Fig. 3D interactive model of the *Limulus polyphemus* pushing leg, as modelled from iodine staining and micro-CT-scanning.
(PDF)

S6 Fig. 3D interactive model of the *Limulus polyphemus* chilaria, as modelled from iodine staining and micro-CT-scanning.
(PDF)

S7 Fig. 3D interactive model of the *Limulus polyphemus* genital operculum, as modelled from iodine staining and micro-CT-scanning.
(PDF)

S8 Fig. 3D interactive model of the *Limulus polyphemus* gill operculum, as modelled from iodine staining and micro-CT-scanning.
(PDF)

Acknowledgments

We would like to thank: Dean Woods and Malcolm Lambert for granting us access to the chemicals needed for iodine staining; Vera Weisbecker for her information on approaches to

iodine staining; and Jason Dunlop and an anonymous referee for their helpful reviews. This research is supported by funding from an Australian Postgraduate Award (to RDCB) and an Australian Research Council Future Fellowship (FT120100770 to JRP).

Author Contributions

Data curation: Russell D. C. Bicknell.

Formal analysis: Russell D. C. Bicknell, Ada J. Klinkhamer, Richard J. Flavel.

Funding acquisition: John R. Paterson.

Investigation: Russell D. C. Bicknell, Richard J. Flavel.

Methodology: Russell D. C. Bicknell, Ada J. Klinkhamer, Richard J. Flavel.

Project administration: Russell D. C. Bicknell.

Resources: Russell D. C. Bicknell.

Supervision: Stephen Wroe, John R. Paterson.

Visualization: Russell D. C. Bicknell, Ada J. Klinkhamer, Richard J. Flavel, John R. Paterson.

Writing – original draft: Russell D. C. Bicknell, Ada J. Klinkhamer, Richard J. Flavel.

Writing – review & editing: Russell D. C. Bicknell, Ada J. Klinkhamer, Richard J. Flavel, Stephen Wroe, John R. Paterson.

References

1. Lautenschlager S, Bright JA, Rayfield EJ. Digital dissection–using contrast-enhanced computed tomography scanning to elucidate hard-and soft-tissue anatomy in the Common Buzzard *Buteo buteo*. Journal of Anatomy. 2014; 224(4): 412–31. https://doi.org/10.1111/joa.12153 PMID: 24350638
2. Fernández R, Kvist S, Lenihan J, Giribet G, Ziegler A. *Sine systemate chaos*? A versatile tool for earthworm taxonomy: non-destructive imaging of freshly fixed and museum specimens using micro-computed tomography. PloS ONE. 2014; 9(5): e96617. https://doi.org/10.1371/journal.pone.0096617 PMID: 24837238
3. Holliday CM, Tsai HP, Skiljan RJ, George ID, Pathan S. A 3D interactive model and atlas of the jaw musculature of *Alligator mississippiensis*. PloS ONE. 2013; 8(6): e62806. https://doi.org/10.1371/journal.pone.0062806 PMID: 23762228
4. Ziegler A, Faber C, Mueller S, Bartolomaeus T. Systematic comparison and reconstruction of sea urchin (Echinoidea) internal anatomy: a novel approach using magnetic resonance imaging. BMC Biology. 2008; 6(1): 33. https://doi.org/10.1186/1741-7007-6-33 PMID: 18651948
5. Ruthensteiner B, Heß M. Embedding 3D models of biological specimens in PDF publications. Microscopy Research and Technique. 2008; 71(11): 778–786. https://doi.org/10.1002/jemt.20618 PMID: 18785246
6. Sharp AC, Trusler PW. Morphology of the jaw-closing musculature in the common wombat (*Vombatus ursinus*) using digital dissection and magnetic resonance imaging. PloS ONE. 2015; 10(2): e0117730. https://doi.org/10.1371/journal.pone.0117730 PMID: 25707001
7. Deans AR, Mikó I, Wipfler B, Friedrich F. Evolutionary phenomics and the emerging enlightenment of arthropod systematics. Invertebrate Systematics. 2012; 26(3): 323–330.
8. Quayle MR, Barnes DG, Kaluza OL, McHenry CR. An interactive three dimensional approach to anatomical description—the jaw musculature of the Australian laughing kookaburra (*Dacelo novaeguineae*). PeerJ. 2014; 2: e355. https://doi.org/10.7717/peerj.355 PMID: 24860694
9. Padial JM, Miralles A, De la Riva I, Vences M. The integrative future of taxonomy. Frontiers in Zoology. 2010; 7(1): 16.
10. Ziegler A, Kunth M, Mueller S, Bock C, Pohmann R, Schröder L, et al. Application of magnetic resonance imaging in zoology. Zoomorphology. 2011; 130(4): 227–254.

11. Lehmann T, Heß M, Melzer RR. Wiring a periscope–ocelli, retinula axons, visual neuropils and the ancestrality of sea spiders. PloS ONE. 2012; 7(1): e30474. https://doi.org/10.1371/journal.pone.0030474 PMID: 22279594
12. Pohlmann A, Möller M, Decker H, Schreiber WG. MRI of tarantulas: morphological and perfusion imaging. Magnetic Resonance Imaging. 2007; 25(1): 129–135. https://doi.org/10.1016/j.mri.2006.08.019 PMID: 17222724
13. Bock C, Frederich M, Wittig R-M, Pörtner H-O. Simultaneous observations of haemolymph flow and ventilation in marine spider crabs at different temperatures: a flow weighted MRI study. Magnetic Resonance Imaging. 2001; 19(8): 1113–1124. PMID: 11711236
14. Baeumler N, Haszprunar G, Ruthensteiner B. 3D interactive microanatomy of *Omalogyra atomus* (Philippi, 1841)(Gastropoda). Zoosymposia. 2008; 1(1): 101–118.
15. Neusser TP, Heß M, Schrödl M. Tiny but complex-interactive 3D visualization of the interstitial acochlidian gastropod *Pseudunela cornuta* (Challis, 1970). Frontiers in Zoology. 2009; 6(1): 20. https://doi.org/10.1186/1742-9994-6-20 PMID: 19747373
16. Haszprunar G, Speimann E, Hawe A, Heß M. Interactive 3D anatomy and affinities of the Hyalogyrinidae, basal Heterobranchia (Gastropoda) with a rhipidoglossate radula. Organisms Diversity & Evolution. 2011; 11(3): 201–236.
17. Brenzinger B, Padula V, Schrödl M. Insemination by a kiss? Interactive 3D-microanatomy, biology and systematics of the mesopsammic cephalaspidean sea slug *Pluscula cuica* Marcus, 1953 from Brazil (Gastropoda: Euopisthobranchia: Philinoglossidae). Organisms Diversity & Evolution. 2013; 13(1):33–54.
18. Vortsepneva E, Ivanov D, Purschke G, Tzetlin A. Morphology of the jaw apparatus in 8 species of Patellogastropoda (Mollusca, Gastropoda) with special reference to *Testudinalia tesulata* (Lottiidae). Zoomorphology. 2013; 132(4): 359–377.
19. Grabe V, Strutz A, Baschwitz A, Hansson BS, Sachse S. Digital *in vivo* 3D atlas of the antennal lobe of *Drosophila melanogaster*. Journal of Comparative Neurology. 2015; 523(3): 530–544. https://doi.org/10.1002/cne.23697 PMID: 25327641
20. Michels J, Gorb S. Detailed three-dimensional visualization of resilin in the exoskeleton of arthropods using confocal laser scanning microscopy. Journal of Microscopy. 2012; 245(1): 1–16. https://doi.org/10.1111/j.1365-2818.2011.03523.x PMID: 22142031
21. Wipfler B, Machida R, Mueller B, Beutel RG. On the head morphology of Grylloblattodea (Insecta) and the systematic position of the order, with a new nomenclature for the head muscles of *Dicondylia*. Systematic Entomology. 2011; 36(2): 241–266.
22. Beutel RG, Friedrich F, Whiting MF. Head morphology of *Caurinus* (Boreidae, Mecoptera) and its phylogenetic implications. Arthropod Structure & Development. 2008; 37(5): 418–433.
23. Klaus A, Kulasekera V, Schawaroch V. Three-dimensional visualization of insect morphology using confocal laser scanning microscopy. Journal of Microscopy. 2003; 212(2): 107–121.
24. Ruthensteiner B, Schröpel V, Haszprunar G. Anatomy and affinities of *Micropilina minuta* Warén, 1989 (Monoplacophora: Micropilinidae). Journal of Molluscan Studies. 2010; 76(4): 323–332.
25. Faulwetter S, Vasileiadou A, Kouratoras M, Dailianis T, Arvanitidis C. Micro-computed tomography: Introducing new dimensions to taxonomy. ZooKeys. 2013;(263): 1–45. https://doi.org/10.3897/zookeys.263.4261 PMID: 23653515
26. Gerhart SD. A review of the biology and management of horseshoe crabs, with emphasis on Florida populations. Fish and Wildlife Research Institute Technical Report TR-12. ii + 24 p.
27. Shultz JW. Gross muscular anatomy of *Limulus polyphemus* (Xiphosura, Chelicerata) and its bearing on evolution in the Arachnida. Journal of Arachnology. 2001; 29(3): 283–303.
28. Metscher BD. MicroCT for comparative morphology: simple staining methods allow high-contrast 3D imaging of diverse non-mineralized animal tissues. BMC Physiology. 2009; 9(1): 1. https://doi.org/10.1186/1472-6793-9-11 PMID: 19545439
29. Gignac PM, Kley NJ. Iodine-enhanced micro-CT imaging: Methodological refinements for the study of the soft-tissue anatomy of post-embryonic vertebrates. Journal of Experimental Zoology (Molecular and Developmental Evolution). 2014; 322B(3): 166–176.
30. Ward DV. Leg extension in *Limulus*. The Biological Bulletin. 1969; 136(2): 288–300.
31. Lankester ER. *Limulus* an Arachnid. Quarterly Journal of Microscopical Science 1881; 23: 504–649.
32. Hayes WF, Barber SB. Proprioceptor distribution and properties in *Limulus* walking legs. Journal of Experimental Zoology. 1967; 165(2): 195–210.
33. Shultz JW. Morphology of locomotor appendages in Arachnida: evolutionary trends and phylogenetic implications. Zoological Journal of the Linnean Society. 1989; 97(1): 1–56.

34. Van der Hammen L. Comparative studies in Chelicerata IV. Apatellata, Arachnida, Scorpionida, Xiphosura. Zoologische Verhandelingen. 1986; 226(28): 1–52.
35. Scholl G. Beiträge zur Embryonalentwicklung von *Limulus* Polyphemus L. (Chelicerata, Xiphosura). Zoomorphologie. 1977; 86(2): 99–154.
36. Lautenschlager S. Palaeontology in the third dimension: a comprehensive guide for the integration of three-dimensional content in publications. Paläontologische Zeitschrift. 2014; 88(1): 111–121.
37. Wyse GA. Central pattern generation underlying *Limulus* rhythmic behavior patterns. Current Zoology. 2010; 56(5): 537–549.
38. Smith SA, Berkson J. Laboratory culture and maintenance of the horseshoe crab (*Limulus polyphemus*). Lab Animal. 2005; 34(7): 27–34. https://doi.org/10.1038/laban0705-27 PMID: 15995694
39. Botton M, Shuster CN Jr, Keinath J. Horseshoe Crabs in a food web: who eats whom. In: Shuster CN Jr., Barlow R, Brockmann H, editors. The American Horseshoe Crab Harvard University Press, Cambridge; 2003. pp. 133–153.
40. Dunlop JA, Lamsdell JC. Segmentation and tagmosis in Chelicerata. Arthropod Structure & Development. 2016; 46(3): 395–418.
41. Battelle B.-A. The eyes of *Limulus polyphemus* (Xiphosura, Chelicerata) and their afferent and efferent projections. Arthropod Structure & Development. 2006; 35(4): 261–274.
42. Yamasaki T, Makioka T, Saito J. Morphology. In: Sekiguchi K, editor. Biology of Horseshoe Crabs. Tokyo: Science House Co.; 1988. pp. 69–132.
43. Dietl J, Nascimento C, Alexander R. Influence of ambient flow around the Horseshoe Crab *Limulus polyphemus* on the distribution and orientation of selected epizoans. Estuaries. 2000; 23(4): 509–520.
44. Yamasaki T. Taxonomy. In: Sekiguchi K, editor. Biology of Horseshoe Crabs. Tokyo: Science House Co.; 1988. pp. 10–21.
45. Eagles DA. Tailspine movement and its motor control in *Limulus polyphemus*. Comparative Biochemistry and Physiology. 1973; 46A(2): 391–407.
46. Levine R, Chantler PD, Kensler RW, Woodhead JL. Effects of phosphorylation by myosin light chain kinase on the structure of *Limulus* thick filaments. The Journal of Cell Biology. 1991; 113(3): 563–572. PMID: 2016336
47. Snodgrass RE. A textbook of arthropod anatomy. Cornell University; 1952.
48. Fahrenbach W. Merostomata. In: Harrison F W, and Foelix R F, editors. Microscopic Anatomy of Invertebrates v. 8A: Chelicerate Arthropoda: New York, Wiley-Liss 1999. pp. 21–115.
49. Botton M. Diet and food preferences of the adult horseshoe crab *Limulus polyphemus* in Delaware Bay, New Jersey, USA. Marine Biology. 1984; 81(2): 199–207.
50. Wyse GA. Receptor organization and function in *Limulus* chelae. Zeitschrift für vergleichende Physiologie. 1971; 73(3): 249–273.
51. Manton SM. Mandibular mechanisms and the evolution of arthropods. Philosophical Transactions of the Royal Society of London B: Biological Sciences. 1964; 247(737): 1–183.
52. Pringle J. Proprioception in *Limulus*. Journal of Experimental Biology. 1956; 33(4): 658–667.
53. Owen R. On the anatomy of the American King-crab (*Limulus polyphemus*, Latr.). Transactions of the Linnean Society of London. 1872; 28(3): 459–506.
54. Fourtner C, Sherman R. A light and electron microscopic examination of muscles in the walking legs of the horseshoe crab, *Limulus polyphemus* (L.). Canadian Journal of Zoology. 1972; 50(11): 1447–1455.
55. Barthel KW. *Limulus*: a living fossil. Naturwissenschaften. 1974; 61(10): 428–433.
56. Suzuki Y, Kondo A, Bergström J. Morphological requirements in limulid and decapod gills: A case study in deducing the function of lamellipedian exopod lamellae. Acta Palaeontologica Polonica. 2008; 53(2): 275–283.
57. Zacaï A, Vannier J, Lerosey-Aubril R. Reconstructing the diet of a 505-million-year-old arthropod: *Sidneyia inexpectans* from the Burgess Shale fauna. Arthropod Structure & Development. 2015; 45(2): 200–220.
58. Selden P.A. Functional morphology of the prosoma of *Baltoeurypterus tetragonophthalmus* (Fischer) (Chelicerata: Eurypterida). Transactions of the Royal Society of Edinburgh: Earth Sciences. 1981; 72 (1): 9–48.
59. Engelhorn T, Eyupoglu IY, Schwarz MA, Karolczak M, Bruenner H, Struffert T, et al. In vivo micro-CT imaging of rat brain glioma: a comparison with 3T MRI and histology. Neuroscience Letters. 2009; 458 (1): 28–31. https://doi.org/10.1016/j.neulet.2009.04.033 PMID: 19379792
60. Godfray HCJ. Challenges for taxonomy. Nature. 2002; 417(6884): 17–19. https://doi.org/10.1038/417017a PMID: 11986643

61. Godfray HCJ, Clark B, Kitching I, Mayo S, Scoble M. The web and the structure of taxonomy. Systematic Biology. 2007; 56(6): 943–955. https://doi.org/10.1080/10635150701777521 PMID: 18066929

62. Xavier JC, Allcock AL, Cherel Y, Lipinski MR, Pierce GJ, Rodhouse PG, et al. Future challenges in cephalopod research. Journal of the Marine Biological Association of the United Kingdom. 2015; 95(5): 999–1015.

Higher Degree Research Thesis by Publication

University of New England

STATEMENT OF ORIGINALITY

(To appear at the end of each thesis chapter submitted as an article/paper)

We, the Research Master/PhD candidate and the candidate's Principal Supervisor, certify that the following text, figures and diagrams are the candidate's original work.

Type of work	Page number/s
Scientific publication	67–89

Name of Candidate: Russell D. C. Bicknell

Name/title of Principal Supervisor: John R. Paterson

_____ 11/04/2019

Candidate Date

_____ 11/04/2019

Principal Supervisor Date

Higher Degree Research Thesis by Publication
University of New England

STATEMENT OF AUTHORS' CONTRIBUTION

(To appear at the end of each thesis chapter submitted as an article/paper)

We, the Research Master/PhD candidate and the candidate's Principal Supervisor, certify that all co-authors have consented to their work being included in the thesis and they have accepted the candidate's contribution as indicated in the *Statement of Originality*.

	Author's Name (please print clearly)	**% of contribution**
Candidate	Russell D. C. Bicknell	60
Other Authors	Ada J. Klinkhamer	10
	Richard J. Flavel	10
	Stephen Wroe	10
	John R. Paterson	10

Name of Candidate: Russell D. C. Bicknell

Name/title of Principal Supervisor: John R. Paterson

_____ 11/04/2019
Candidate Date

_____ 11/04/2019
Principal Supervisor Date

Paper 4

Computational biomechanical analyses demonstrate similar shell-crushing abilities in modern and ancient arthropods

Higher Degree Research Thesis by Publication
University of New England

STATEMENT OF ORIGINALITY

(To appear at the end of each thesis chapter submitted as an article/paper)

We, the Research Master/PhD candidate and the candidate's Principal Supervisor, certify that the following text, figures and diagrams are the candidate's original work.

Type of work	Page number/s
Scientific publication	95–102

Name of Candidate: Russell D. C. Bicknell

Name/title of Principal Supervisor: John R. Paterson

Candidate — 11/04/2019 Date

Principal Supervisor — 11/04/2019 Date

Higher Degree Research Thesis by Publication
University of New England

STATEMENT OF AUTHORS' CONTRIBUTION

(To appear at the end of each thesis chapter submitted as an article/paper)

We, the Research Master/PhD candidate and the candidate's Principal Supervisor, certify that all co-authors have consented to their work being included in the thesis and they have accepted the candidate's contribution as indicated in the *Statement of Originality*.

	Author's Name (please print clearly)	**% of contribution**
Candidate	Russell D. C. Bicknell	50
Other Authors	Justin A. Ledogar	10
	Stephen Wroe	10
	Benjamin C. Gutzler	5
	Winsor H. Watson III	5
	John R. Paterson	20

Name of Candidate: Russell D. C. Bicknell

Name/title of Principal Supervisor: John R. Paterson

[redacted]

_____ 11/04/2019
Candidate Date

[redacted]

_____ 11/04/2019
Principal Supervisor Date

Paper 5

Abnormal xiphosurids, with possible application to Cambrian trilobites

Higher Degree Research Thesis by Publication
University of New England

STATEMENT OF ORIGINALITY

(To appear at the end of each thesis chapter submitted as an article/paper)

We, the Research Master/PhD candidate and the candidate's Principal Supervisor, certify that the following text, figures and diagrams are the candidate's original work.

Type of work	Page number/s
Scientific publication	107–123

Name of Candidate: Russell D. C. Bicknell

Name/title of Principal Supervisor: John R. Paterson

_____ 11/04/2019
Candidate Date

_____ 11/04/2019
Principal Supervisor Date

Higher Degree Research Thesis by Publication
University of New England

STATEMENT OF AUTHORS' CONTRIBUTION

(To appear at the end of each thesis chapter submitted as an article/paper)

We, the Research Master/PhD candidate and the candidate's Principal Supervisor, certify that all co-authors have consented to their work being included in the thesis and they have accepted the candidate's contribution as indicated in the *Statement of Originality*.

	Author's Name (please print clearly)	**% of contribution**
Candidate	Russell D. C. Bicknell	65
Other Authors	Stephen Pates	25
	Mark L. Botton	10

Name of Candidate: Russell D. C. Bicknell

Name/title of Principal Supervisor: John R. Paterson

_____ 11/04/2019
Candidate Date

_____ 11/04/2019
Principal Supervisor Date

Paper 6

Abnormal extant xiphosurids in the Yale Peabody Museum Invertebrate Zoology collection

Abnormal Extant Xiphosurids in the Yale Peabody Museum Invertebrate Zoology Collection

Russell D. C. Bicknell[1] and Stephen Pates[2,3]

[1] *Corresponding author:* Palaeoscience Research Centre, School of Environmental and Rural Science, University of New England, Armidale New South Wales 2351 Australia
—*email:* rdcbicknell@gmail.com

[2] Department of Zoology, University of Oxford, Oxford OX1 3PS United Kingdom

[3] Institute of Earth Sciences, University of Lausanne, Lausanne CH-1015 Switzerland

Abstract

Xiphosurids are an archetypal group of chelicerates with extensive anatomical, physiological, and paleontological documentation. Despite this research, very little information is available concerning abnormal specimens of the group. Here we vastly increase the number of documented abnormal extant xiphosurids by identifying 17 specimens showing a range of abnormalities on the appendages, cephalothorax, thoracetron, and telson. These specimens include all extant species and the first documentation of abnormal *Carcinoscorpius rotundicauda*. We note that previous suggestions that the telson was the most commonly abnormal body part may reflect a species-specific bias and propose increased use of museum collections to understand these iconic organisms and their abnormalities.

Keywords

Abnormalities, Xiphosurida, *Carcinoscorpius rotundicauda*, *Limulus polyphemus*, *Tachypleus gigas*, *Tachypleus tridentatus*

Introduction

True horseshoe crabs (order Xiphosurida within Chelicerata) have been, and continue to be, extensively studied arthropods due to their size and fossil record. The anatomical (e.g., Owen 1872; Lankester 1881; Shultz 2001; Bicknell, Klinkhamer et al. 2018; Bicknell, Paterson et al. 2018), biochemical (e.g., Kaplan et al. 1977), biomechanical (Bicknell, Ledogar et al. 2018), ecological (e.g., Sokoloff 1978; Shuster 1982; Shuster and Sekiguchi 2009; Fairuz-Fozi et al. 2018), genetic (e.g., Sokoloff 1978; Obst et al. 2012), and paleontological (e.g., Woodward 1879; Fisher 1984; Selden and Siveter 1987; Hauschke and Wilde 1991; Lamsdell 2013, 2016; Bicknell, Pates et al. 2018) facets of horseshoe crabs have therefore been thoroughly documented. Recent research (Bicknell, Pates et al. 2018) highlighted that extant and extinct horseshoe crab abnormalities are underexplored. Bicknell, Pates et al. (2018) presented notes on all previously documented abnormal specimens (see van der Meer Mohr 1935; Shuster 1982; Jell 1989 for the majority of other abnormalities) and demonstrated abnormalities in both extant and extinct species. Using specimens in the Division of Invertebrate Zoology collection in the Peabody Museum of Natural History, Yale University, here we further this work by reporting abnormalities on all extant xiphosurid species: *Carcinoscorpius rotundicauda* (Latreille, 1802), the mangrove horseshoe crab sensu Cartwright-Taylor et al. (2009); *Limulus polyphemus* (Linnaeus, 1758), the Atlantic or American horseshoe crab, sensu Shuster et al. (2003); *Tachypleus gigas* (Müller, 1785), the South Asian horseshoe crab, sensu Miyata et al. (1984); and *Tachypleus tridentatus* (Leach, 1819), the Japanese horseshoe crab sensu Nakamura et al. (1976). In doing so, we present new examples of abnormalities (including an apparently rare abnormal appendage) and the first documented examples of abnormalities in *C. rotundicauda*.

Abnormalities: Causes and Forms

Following Owen (1985) and Bicknell, Pates et al. (2018), the term *abnormality* describes a misshapen or missing exoskeletal section, or an additional and unusual growth. Although original causes may be unknown, three major abnormality-inducing pathways have been suggested: injuries, teratologies and pathologies (Bicknell, Pates et al. 2018 modified the definitions in Owen 1985—originally applied to trilobites—to xiphosurid abnormalities).

Injuries are the result of mechanical damage induced by predators, or self-inflicted accidentally during molting, mating or burrowing. These are generally V-, W-, U- or L-shaped embayments or indents in the xiphosuran exoskeleton. Scar formation (cicatrisation) occurs at injury site, with partial regeneration of injured areas during subsequent molting events. Injuries can affect one side of the exoskeleton (unilateral) or both sides thereof (bilateral). Teratologies are developmental and genetic aberrations and can result in the additional, abnormal or failed growth of spines and body parts (e.g., segments, spines). Pathologies are atrophied tissue caused by disease, or abnormal growth of exoskeleton around a parasitic intrusion.

Methods

This approach develops on Jell (1989) and Bicknell, Pates et al. (2018), who reported abnormal specimens from museum collections. All dry and wet xiphosurid specimens from the Division of Invertebrate Zoology, Peabody Museum of Natural History, Yale University, New Haven, Connecticut, USA (YPM IZ), collection were reviewed for abnormalities ($n = 127$). Abnormal specimens were photographed with a Canon D60 under LED (light-emitting diode) lighting in the Yale Peabody Museum's Division of Invertebrate Paleontology. Wet specimens were removed from alcohol and imaged. Images were stacked using Helicon Focus 6 (Helicon Soft Limited) stacking software. Injured trilobite specimens from Cambrian-aged deposits displaying recovering thoracic spines from the South Australia Museum, Adelaide, Australia (SAM), and Museo de Ciencias Naturales de la Universidad de Zaragoza, Zaragoza, Spain (MPZ), were presented for comparison with one of the thoracetronic abnormalities.

Results

Carcinoscorpius rotundicauda

A total of 14 *Carcinoscorpius rotundicauda* specimens were reviewed, and four adult specimens with abnormalities to the cephalothorax, thoracetron and telson were documented. The first specimen (YPM IZ 103383) shows a bilaterally expressed cephalothoracic abnormality with W-shaped indentations on both genal spines (Figure 1A, C, D). The second specimen (YPM IZ 055595) has a symmetrical U-shaped indentation on the posterior right thoracetron (Figure 1B, E). The right thoracetron side has five moveable spine notches, one fewer than the left side. The third specimen (YPM IZ 103384) displays an asymmetric U-shaped indentation on the anterior right thoracetron and one fewer movable spine on the right side (four) than the left (five) (Figure 2A, B). The fourth specimen (YPM IZ 055594) has a kink within the last fifth of the telson (Figure 2C, D).

Limulus polyphemus

A total of 88 *Limulus polyphemus* specimens were reviewed. A juvenile specimen (YPM IZ 103398) is the only abnormal wet specimen and has a stunted, left-curved telson (Figure 3D, E). Another specimen (YPM IZ 030231) has an injured thoracetron and telson (Figure 3A–C). The thoracetron has a W-shaped indentation in the middle-left side, and lacks a moveable spine and the associated spine notch (Figure 3A, C). The telson has a slight kink in the last third of the tail-spine (Figure 3A, B). The largest *L. polyphemus* specimen in the Yale Peabody Museum collection (YPM IZ 055601; approximately 52 cm long) has a kink in the first third of the telson (Figure 4A, B) and movable spines on the right posterior thoracetron that are a third the size of spines on the left side (Figure 4A, D). Only one specimen (YPM IZ 055579) is documented here with an appendage abnormality: a shortened apotele on the right pushing leg (cephalothoracic appendage VI) (Figure 4C, E).

Tachypleus gigas

A total of 17 *Tachypleus gigas* specimens were reviewed. Six abnormal, adult *T. gigas* specimens were documented: five with cephalothoracic abnormalities, and one with a thoracetronic

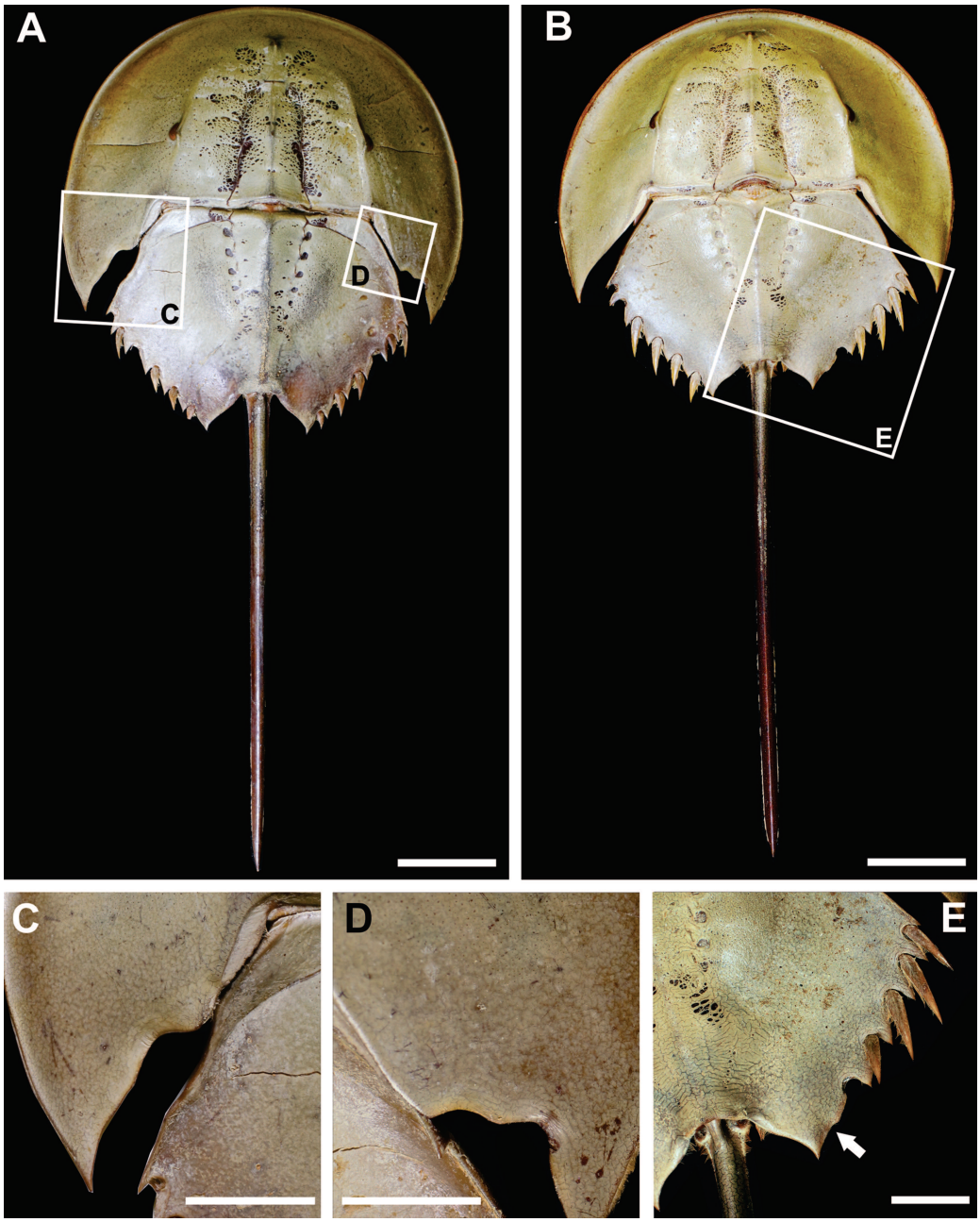

FIGURE 1. *Carcinoscorpius rotundicauda* specimens with cephalothoracic and thoracetronic abnormalities. **A.** *Carcinoscorpius rotundicauda* with W-shaped indentation to both genal spines (YPM IZ 103383). **B.** *Carcinoscorpius rotundicauda* with U-shaped indentation in thoracetron (YPM IZ 055595). **C.** Close-up of indentation to left genal spine (YPM IZ 103383). **D.** Close-up of indentation to right genal spine (YPM IZ 103383). **E.** Close-up of indentation in thoracetron (YPM IZ 055595; white arrow). All images in dorsal view. Scale bars equal 3 cm (A, B) and 1.5 cm (C–E).

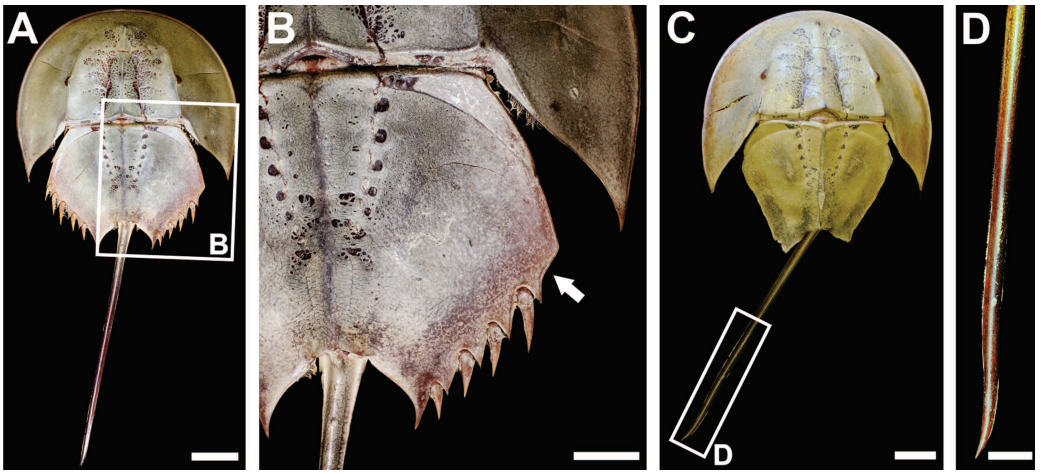

FIGURE 2. *Carcinoscorpius rotundicauda* specimens with thoracetronic and telson abnormalities. **A, B.** *Carcinoscorpius rotundicauda* with U-shaped indentation on thoracetron (YPM IZ 103384). **B.** Close-up of indentation in A (white arrow). **C, D.** *Carcinoscorpius rotundicauda* with kinked telson (YPM IZ 055594). **D.** Close-up of telson. All images in dorsal view. Scale bars equal 3 cm (A), 1.5 cm (B), 2 cm (C) and 0.5 cm (D).

abnormality. This species had the most diverse range of abnormality shapes in the collection. The first specimen (YPM IZ 103380) displays an abnormal left cephalothoracic genal spine with a W-shaped injury comparable to the embayment in a *Carcinoscorpius rotundicauda* specimen (Figure 1A, C, D) and a small, oval-shaped indentation (Figure 5A, D). The second specimen (YPM IZ 055599) shows a rounded genal spine with a protrusion developing dorsally from the rounded edge (Figure 5B, F). The third specimen (YPM IZ 103366) has an O-shaped impression on the left anterior cephalothorax that deformed the surrounding exoskeleton (Figure 5C, E). The fourth specimen (YPM IZ 103369) displays two injuries to the right cephalothorax (Figure 6A, D, E). The cephalothoracic border has a small U-shaped embayment on the right anterior section (Figure 6A, D) and the posterior right genal spine has two terminal points (Figure 6A, E). The fifth specimen (YPM IZ 103382) possesses a large U-shaped indentation on the center-left cephalothorax (Figure 6B, F). This indentation is coupled with an ovate hole located dorsally above from the indentation. The hole has evidence of recovery. The only *T. gigas* specimen with a thoracetronic abnormality was a female specimen (YPM IZ 103377; Figure 6C and G). This specimen has five moveable spine notches on the right side, as opposed to six, and two moveable spines developed in the fourth notch (Figure 6G).

Tachypleus tridentatus

A total of eight *Tachypleus tridentatus* specimens were reviewed, and three abnormal *T. tridentatus* specimens (two adults, one juvenile) were documented. These displayed cephalothoracic, thoracetronic and telson abnormalities. A large adult specimen (YPM IZ 055581) has a bilateral thoracetronic abnormality (Figure 7A–C). The left thoracetron has a posterior movable spine removed and another stunted moveable spine (Figure 7B). The right thoracetron has two stunted anterior moveable spines, the most anterior of which is fused to the thoracetron (Figure 7C). The other adult specimen (YPM IZ 002430) shows a U-shaped indentation in the left anterior cephalothoracic margin (Figure 7D, E). The juvenile specimen (YPM IZ 103381) has a left-curved telson (Figure 7F, G).

Discussion

Injury is the most common cause of abnormality observed in our study. The W- and U-shaped embayments and indents to cephalothoraxes and thoracetrons are diagnostic of mechanical damage. Only one specimen (YPM IZ 103382) shows

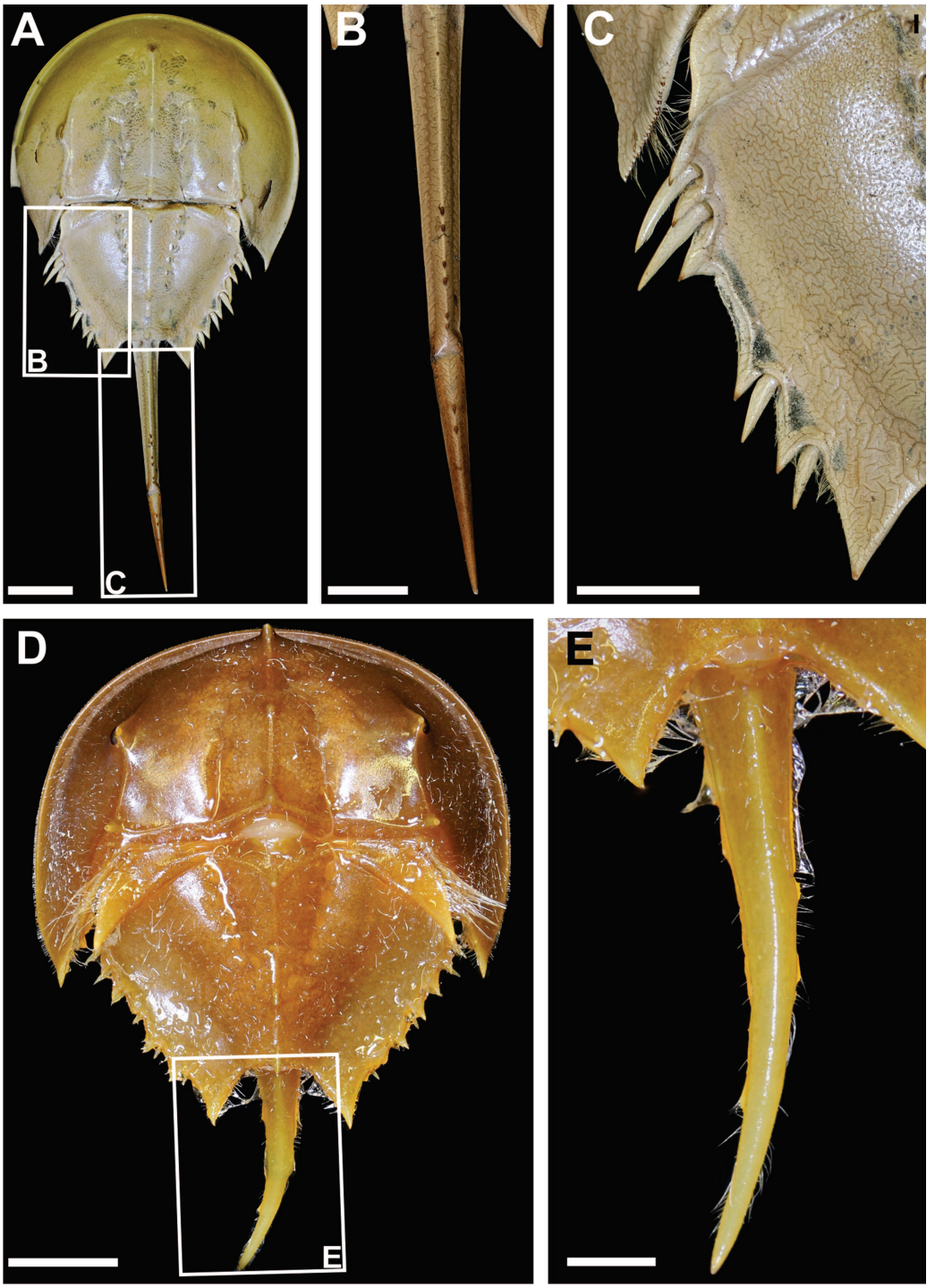

FIGURE 3. *Limulus polyphemus* specimens with thoracetronic and telson abnormalities. **A–C.** *Limulus polyphemus* with kinked telson and abnormal thoracetron (YPM IZ 030231). **B.** Close-up of kinked telson. **C.** Close-up of W-shaped indentation on thoracetron. **D, E.** Juvenile *Limulus polyphemus* (wet specimen) with left-curved telson (YPM IZ 103398). **E.** Close-up of telson. All images in dorsal view. Scale bars equal 3 cm (A), 1.5 cm (B, C), 1 cm (D) and 0.25 cm (E).

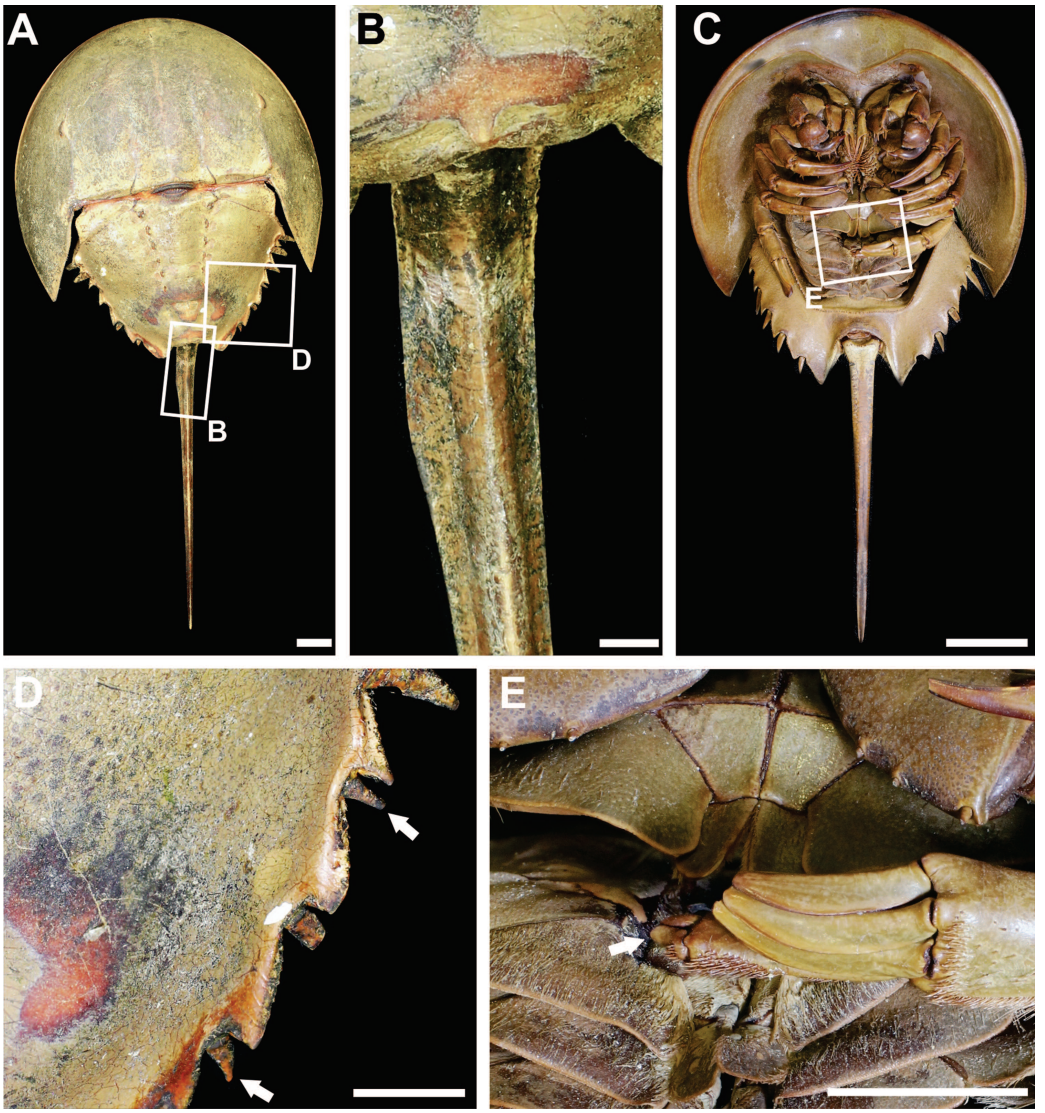

FIGURE 4. *Limulus polyphemus* specimens with abnormal moveable spines, appendages and telsons. **A.** Shortened moveable spines and kinked telson (YPM IZ 055601). **B.** Close-up of kinked telson (YPM IZ 055601). **C.** Abnormal pushing leg (YPM IZ 055579). **D.** Close-up of shortened moveable spines (YPM IZ 055601; white arrows). **E.** Close-up of damaged appendage (YPM IZ 055579; white arrow). A, B, D, in dorsal view. C, E, in ventral view. Scale bars equal 3 cm (A, C), 0.75 cm (B) and 1.5 cm (D, E).

evidence of scarring and recovery, with all other injuries having therefore likely undergone some level of regeneration and therefore multiple molting events. The U shape of some injuries could indicate either an injury from tearing softer exoskeleton after a molting event, or an injury that has undergone substantial recovery, or both. Unequal numbers of movable spines on thoracetron sides and missing spine notches are also evidence of injuries (YPM IZ 030231, YPM IZ 055595 and YPM IZ 103384; Figures 1B, E, 2A, B, and 3A, C). Examples of stunted, absent or otherwise abnormal spines may reflect a teratological cause. The exception to this is a specimen (YPM IZ 103377; Figure 6C, G) in which two spines have developed in one thoracetronic spine notch. This abnormality likely resulted from a previously injured notch. This is similar to the

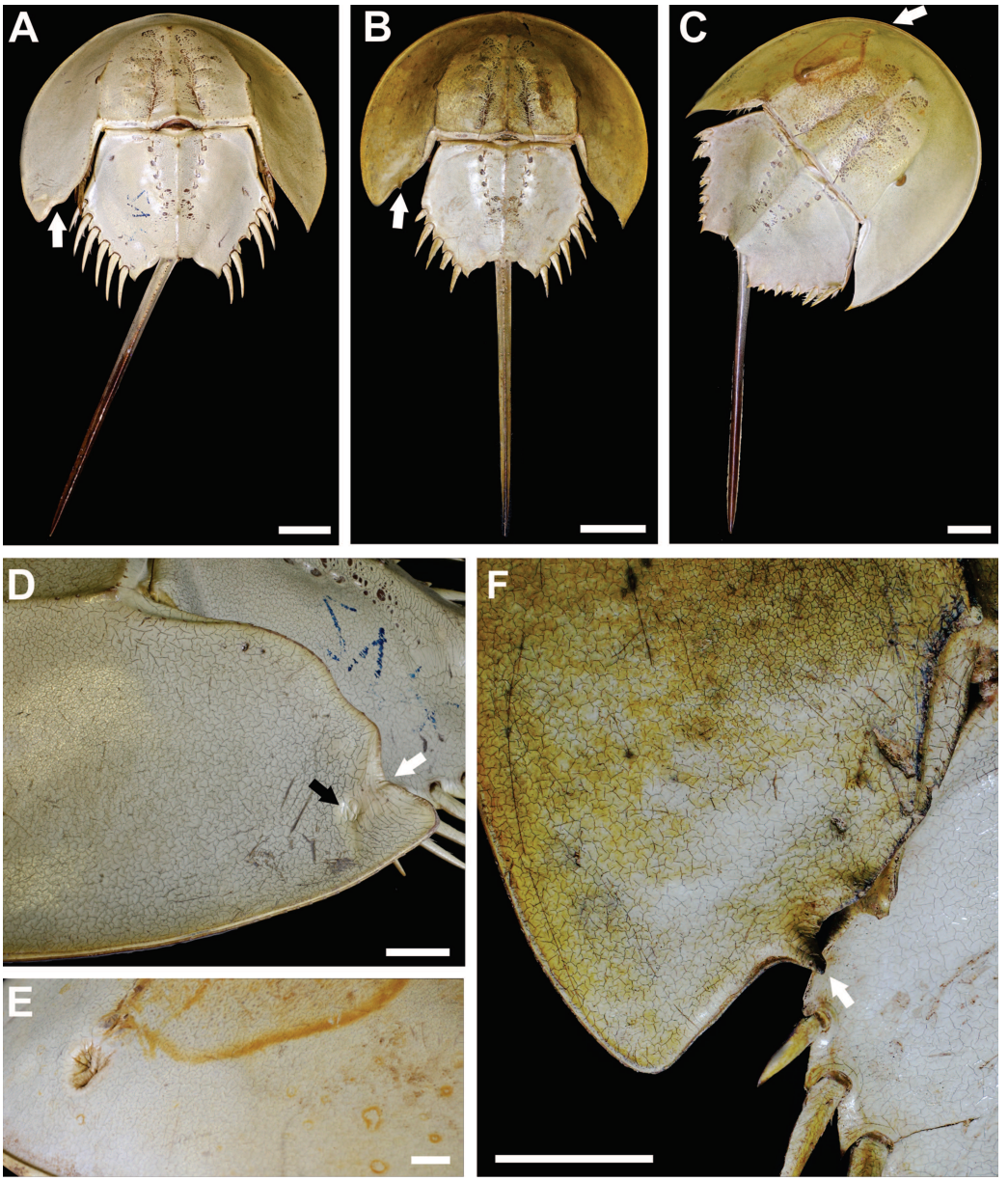

FIGURE 5. *Tachypleus gigas* specimens with abnormal cephalothoraxes. **A.** W-shaped indentation and oval-shaped indentation on left genal spine (YPM IZ 103380). White arrow indicates abnormalities. **B.** Rounded genal spine with protrusion (white arrow; YPM IZ 055599). **C.** O-shaped impression in the left anterior cephalothorax (white arrow; YPM IZ 103366). **D.** Close-up of abnormalities (YPM IZ 103380). White arrow: W-shaped indentation; black arrow: oval-shaped indentation. **E.** Close-up of impression (YPM IZ 103366). **F.** Close-up of protrusion (white arrow; YPM IZ 055599). A–C, F, in dorsal view. D–E, in lateral view. Scale bars equal 3 cm (A–C), 1.5 cm (D, F) and 2 cm (E).

development of two spines from an injured single thoracic section is seen in Cambrian trilobites (Figure 8; Pates et al. 2017). In one case (YPM IZ 103366), the O-shaped impression in the left anterior cephalothorax could be a pathology associated with a parasite.

Shuster (1982), Botton and Loveland (1989) and Bicknell, Pates et al. (2018) all observed that

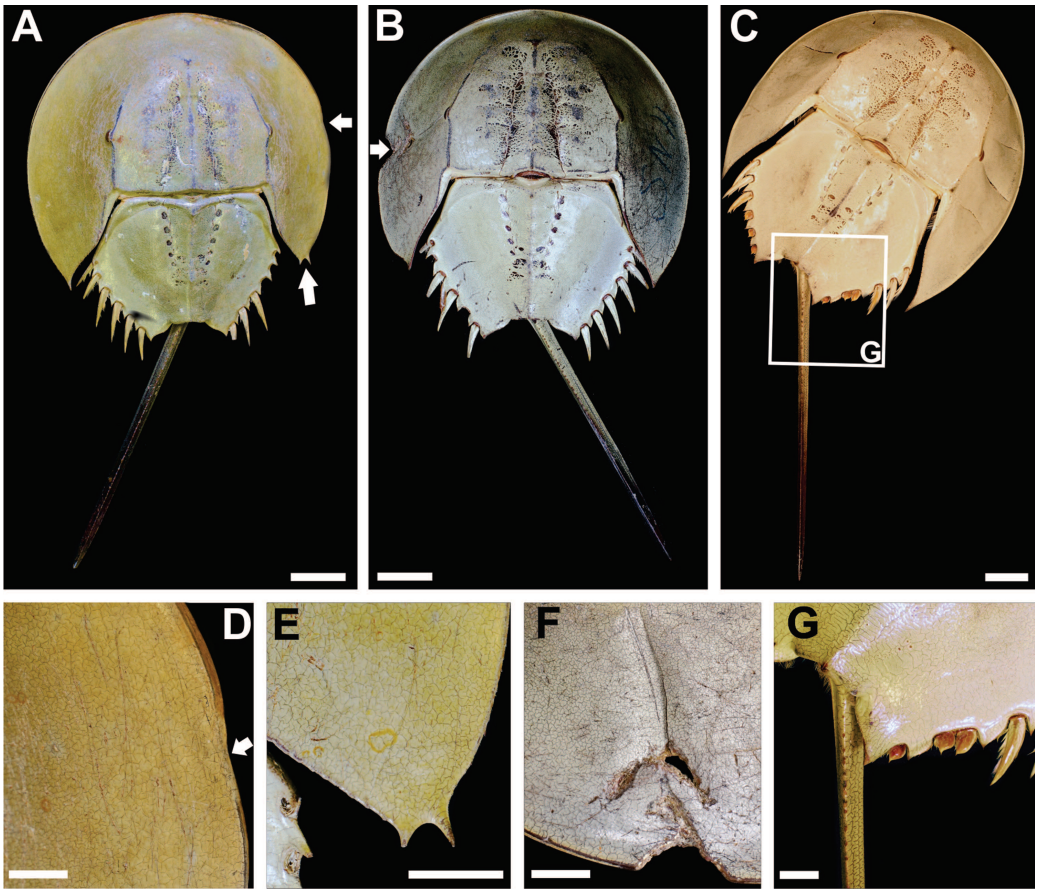

FIGURE 6. *Tachypleus gigas* specimens with abnormal cephalothoraxes and thoracetrons. **A.** U-shaped embayment on right anterior cephalothorax and abnormal right genal spine (white arrows) (YPM IZ 103369). **B.** U-shaped indentation in center-left cephalothorax (white arrow) (YPM IZ 103382). **C.** Female specimen with abnormal right thoracetron (YPM IZ 103377). **D.** Close-up of U-shaped embayment (YPM IZ 103369; white arrow). **E.** Close-up of two genal spine points (YPM IZ 103369). **F.** Close-up of indentation and ovate hole (YPM IZ 103382). Hole is scarred. **G.** Close-up of thoracetron with two moveable spines in the same notch (YPM IZ 103377). A–C, G, in dorsal view. D–F, in lateral view. Scale bars equal 3 cm (A, B), 2 cm (C, F), 1 cm (D, E) and 1.5 cm (G).

telson abnormalities were the most frequently documented horseshoe crab abnormalities. The *Limulus polyphemus* specimens documented here did have more telson abnormalities than other types; however, the three other horseshoe crab species displayed more cephalothoracic and thoracetronic abnormalities (Table 1). In *Tachypleus gigas*, abnormalities were incurred most often on the cephalothorax, whereas in *Carcinoscorpius rotundicauda* and *T. tridentatus* they were found on all sections of the exoskeleton in similar proportions. Patterns of abnormalities in extant horseshoe crabs may therefore be species-specific and could potentially relate to the environmental conditions inhabited by the taxa or predatory groups targeting the different species. As the small sample size presented herein cannot offer conclusive statistical support, a quantitative study of bulk samples considering large populations of all four species is needed to confirm or reject this hypothesis.

Bursey (1977) and Clare et al. (1990) represent the few attempts at intentionally damaging *Limulus polyphemus* specimens to explore how the injuries recovered at a cellular level. However, no attempts have been made to replicate naturally occurring abnormalities in a laboratory. An extension of Clare et al. (1990) could be to inflict injuries

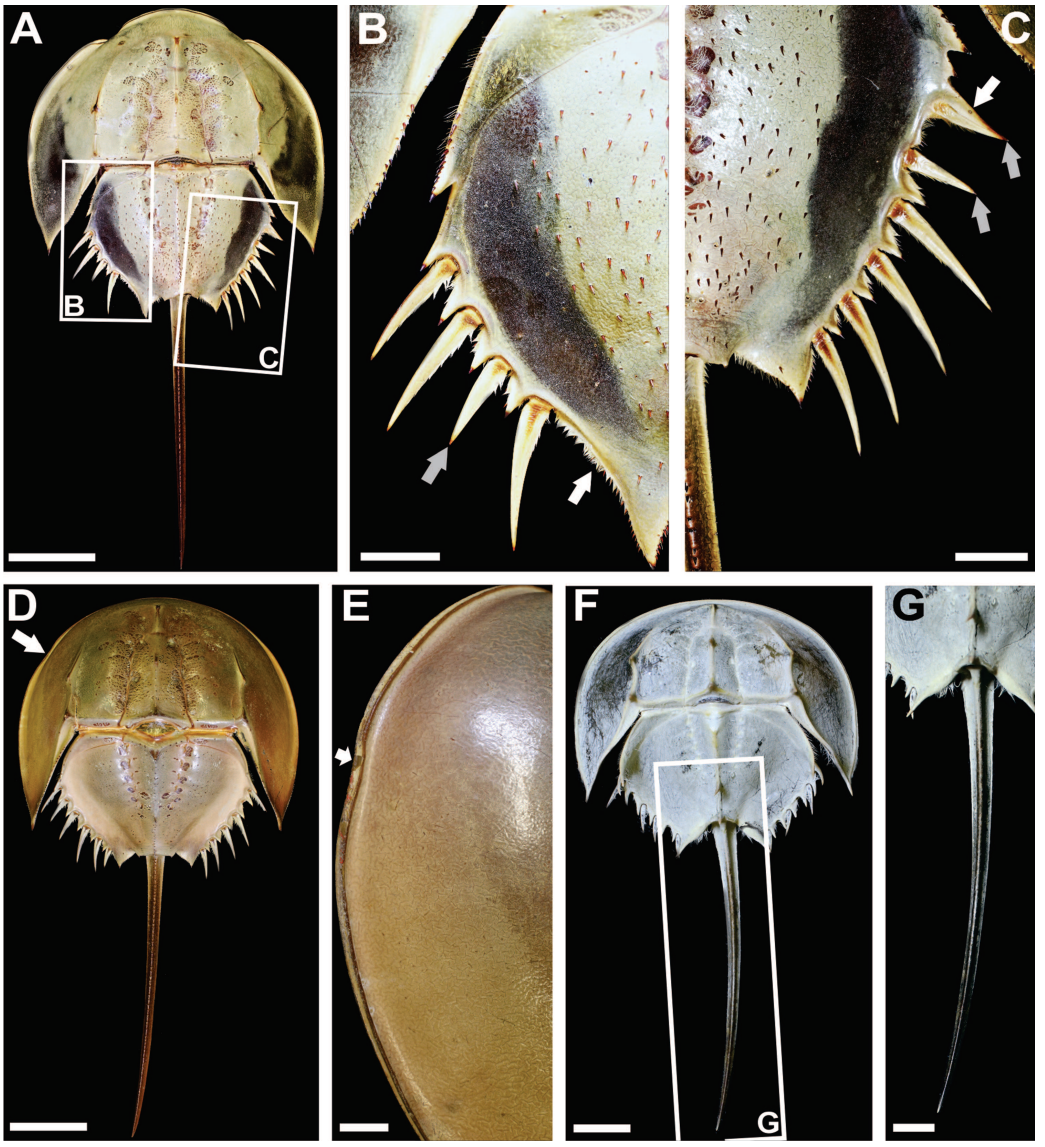

FIGURE 7. *Tachypleus tridentatus* specimen with abnormalities. **A–C.** Specimen with bilateral, thoracetronic abnormalities (YPM IZ 055581). **B.** Left thoracetron with movable spine removed (white arrow) and stunted spine (gray arrow). **C.** Right thoracetron with two stunted moveable spines (gray arrows) and a spine fused to thoracetron (white arrow). **D, E.** U-shaped indentation in the left anterior cephalothorax (white arrow) (YPM IZ 002430). **E.** Close-up of indentation (white arrow). **F, G.** Juvenile with left-curved telson (YPM IZ 103381). **G.** Close-up of telson. A–D, F, G, in dorsal view. E, in lateral view. Scale bars equal 6 cm (A, D), 1.5 cm (B, C), 1 cm (E. F) and 0.5 cm (G).

to specimens raised and housed in a laboratory to document how the individuals recovered at the macro-scale in subsequent molting events. This experiment would allow researchers to determine how horseshoe crab exoskeletons recover from potentially traumatic damage and to suggest the extent of recovery (if any) for naturally produced abnormalities. Furthermore, data on injury recovery across multiple molting events will aid paleontologists interested in understanding how extinct limulids and possibly trilobites recovered from injuries (sensu Pates et al. 2017, fig. 10).

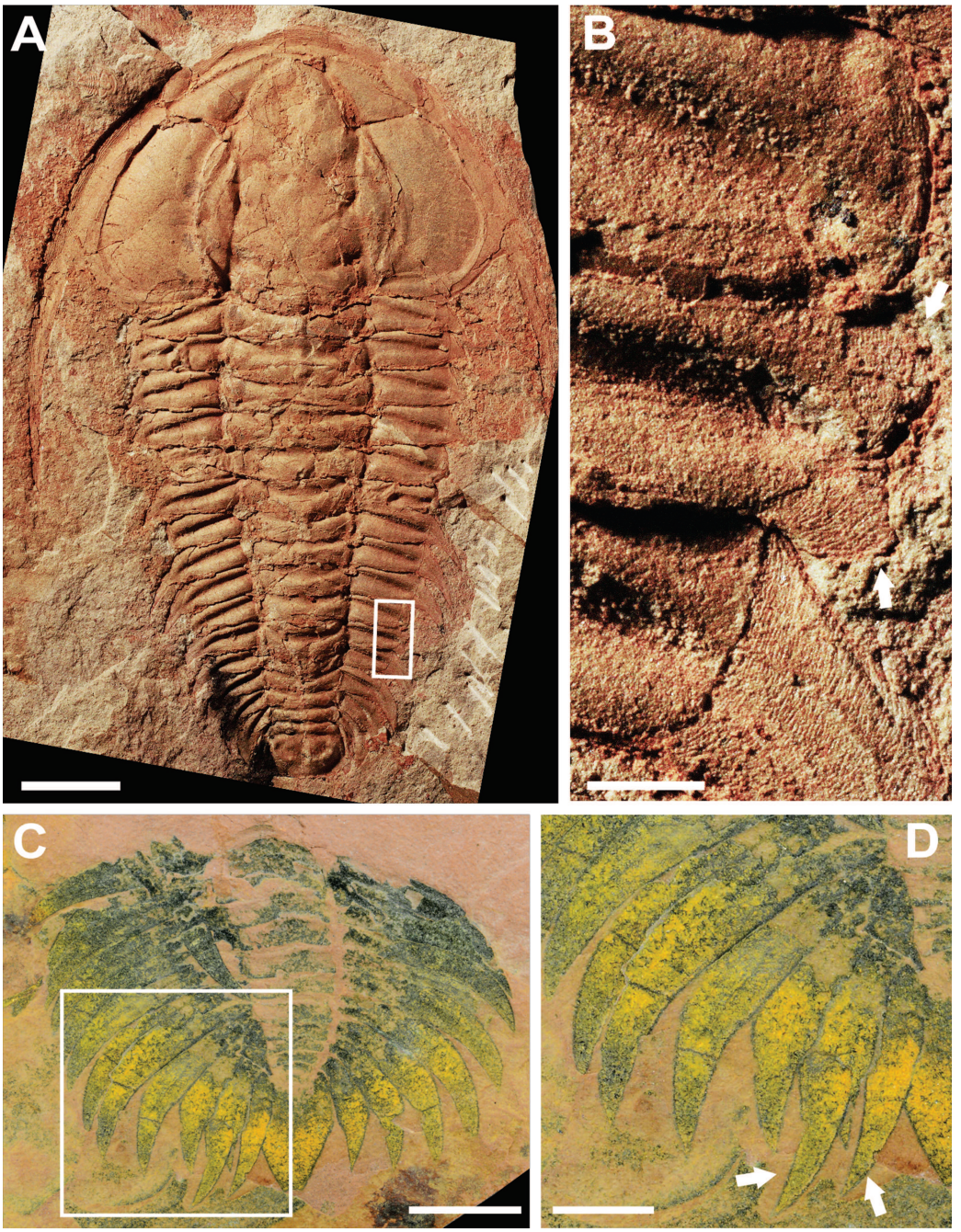

FIGURE 8. Cambrian trilobites with multiple thoracic spines recovering in same thoracic segment. **A, B.** *Redlichia takooensis* Lu, 1950 from lower Cambrian (Series 2, Stage 4) Emu Bay Shale, Kangaroo Island, South Australia (SAM P46038). Two thoracic spines developed in 11th thoracic segment on right side. Area has been injured and produced an L-shaped injury. **B.** Close-up of injury and recovery (white arrows). **C, D.** *Eccaparadoxides pradoanus* (Verneuil and Barrande in Prado et al. 1860) from Purujosa Red Beds, Murero Formation (Miaolingian Series, Drumian), Iberian Chains, Spain (MPZ 2017/1088). Multiple thorax spines developed in 16th and 17th thoracic segments on left side. **D.** Close-up of injury and spine recovery (white arrows). Scale bars equal 1 cm (A, C), 0.125 cm (B) and 0.5 cm (D). Image credit: A, B, courtesy of Russell Bicknell; C, D, courtesy of Samuel Zamora.

TABLE 1. Summary of abnormalities for examined xiphosurid specimens in the Division of Invertebrate Zoology, Yale Peabody Museum of Natural History. For each species, the number of abnormalities in each of the four examined body areas is reported. The total number of specimens of each species in the collection is presented. *Carcinoscorpius rotundicauda* abnormalities were most commonly found on the thoracetron and telson. *Limulus polyphemus* abnormalities were most commonly found on the telson. *Tachypleus gigas* abnormalities were most commonly incurred on the cephalothorax. *Tachypleus tridentatus* had injuries incurred equally on the cephalothorax, thoracetron, and telson.

		Number of abnormalities			
Species	**Specimen counts**	**Cephalothorax**	**Thoracetron**	**Appendages**	**Telson**
Carcinoscorpius rotundicauda	$n = 14$	1	2	0	2
Limulus polyphemus	$n = 88$	0	1	1	3
Tachypleus gigas	$n = 17$	5	1	0	0
Tachypleus tridentatus	$n = 8$	1	1	0	1

Amazing "discoveries [are] made in museum drawers" (Gould 1989:80) as is exemplified by the research within the Smithsonian that sparked the Burgess Shale revolution and restudy of the Cambrian Explosion. Here, we have conducted similar research, an approach that has two important uses: (1) Museum collections often go unconsidered for decades, even though they are often easily accessible, specimen rich and provide diverse records of extant and extinct organisms. (2) These collections aid in the conservation of endangered species. Today, through harvesting for biomedical research and food (Botton 2001; Hsieh and Chen 2009; Akbar John et al. 2011; Nelson et al. 2015; Kwan et al. 2016; Fairuz-Fozi et al. 2018), horseshoe crabs are becoming a threatened group, despite having survived four mass extinctions since their origination early in the Phanerozoic (Størmer 1952, 1955; Selden and Siveter 1987; Rudkin and Young 2009; Van Roy et al. 2010). Museum collections that have been amassed over decades therefore represent one of the best potential avenues for understanding these still enigmatic organisms and have a role to play in recovering stable population levels.

Conclusion

Our study of extant xiphosurids with abnormalities reports 17 new examples of abnormal specimens and the first examples of abnormal *Carcinoscorpius rotundicauda*. The majority of documented abnormalities are considered injuries. Our data suggest that abnormality patterns may be species-specific and potentially reflect environmental or predatory influences. We note that museum collections, such as the Division of Invertebrate Zoology, Yale Peabody Museum, are ideal for further documenting interesting features on these iconic species.

Acknowledgments

This research was supported by funding from an Australian Postgraduate Award (to Bicknell), a Charles Schuchert and Carl O. Dunbar Grants-in-Aid award (to Bicknell) and an Oxford-St Catherine's Brade-Natural Motion Scholarship (to Pates). We thank Susan Butts and Jessica Utrup for use of the Division of Invertebrate Paleontology, Yale Peabody Museum camera. We thank Lourdes Rojas for help with specimens from the Division of Invertebrate Zoology, Yale Peabody Museum. Finally, we thank the editor, Patrick Sweeney, and the two reviewers, Olda Fatka and Daniel Drew, for their useful and supportive comments that helped improve the manuscript.

Received 11 September 2018; revised and accepted 12 October 2018.

Literature Cited

AKBAR JOHN, B.A., K.C.A. JALAL, K. ZALEHA, P. ARMSTRONG AND B.Y. KMARUZZAMAN. 2011. Effects of blood extraction on the mortality of Malaysian horseshoe crabs (*Tachypleus gigas*). Marine and Freshwater Behaviour and Physiology 44(5):321–327.

BICKNELL, R.D.C., A.J. KLINKHAMER, R.J. FLAVEL, S. WROE AND J.R. PATERSON. 2018. A 3D anatomical atlas of appendage

musculature in the chelicerate arthropod *Limulus polyphemus*. PLoS ONE 13(2):e0191400.

Bicknell, R.D.C., J.A. Ledogar, S. Wroe, B.C. Gutzler, W.H. Watson III and J.R. Paterson. 2018. Computational biomechanical analyses demonstrate similar shell-crushing abilities in modern and ancient arthropods. Proceedings of the Royal Society B: Biological Sciences 285(1889):20181935.

Bicknell, R.D.C., J.R. Paterson, J.-B. Caron and C.B. Skovsted. 2018. The gnathobasic spine microstructure of Recent and Silurian chelicerates and the Cambrian artiopodan *Sidneyia*: Functional and evolutionary implications. Arthropod Structure & Development 47(1):12–24.

Bicknell, R.D.C., S. Pates and M.L. Botton. 2018. Abnormal xiphosurids, with possible application to Cambrian trilobites. Palaeontologia Electronica 21(2):1–17.

Botton, M.L. 2001. The conservation of horseshoe crabs: What can we learn from the Japanese experience? In: J.T. Tanacredi, ed. *Limulus* in the Limelight. New York: Springer. pp. 41–51.

Botton, M.L. and R.E. Loveland. 1989. Reproductive risk: High mortality associated with spawning by horseshoe crabs (*Limulus polyphemus*) in Delaware Bay, USA. Marine Biology 101(2):143–151.

Bursey, C.R. 1977. Histological response to injury in the horseshoe crab, *Limulus polyphemus*. Canadian Journal of Zoology 55(7):1158–1165.

Cartwright-Taylor, L., J. Lee and C.C. Hsu. 2009. Population structure and breeding pattern of the mangrove horseshoe crab *Carcinoscorpius rotundicauda* in Singapore. Aquatic Biology 8(1):61–69.

Clare, A.S., G. Lumb, P.A. Clare and J.D. Costlow Jr. 1990. A morphological study of wound response and telson regeneration in postlarval *Limulus polyphemus* (L.). Invertebrate Reproduction & Development 17(1):77–87.

Fairuz-Fozi, N., B. Satyanarayana, N.A.M. Zauki, A.M. Muslim, M.-L. Husain, S. Ibrahim and B.R. Nelson. 2018. *Carcinoscorpius rotundicauda* (Latreille, 1802) population status and spawning behaviour at Pendas coast, Peninsular Malaysia. Global Ecology and Conservation 15:e00422.

Fisher, D.C. 1984. The Xiphosurida: Archetypes of bradytely? In: N. Eldredge and S.M. Stanley, eds. Living Fossils. New York: Springer. pp. 196–213.

Gould, S.J. 1989. Wonderful Life: The Burgess Shale and the Nature of History. New York: W. W. Norton & Company. 347 pp.

Hauschke, N. and V. Wilde. 1991. Zur Verbreitung und Ökologie mesozoischer Limuliden. Neues Jahrbuch für Geologie und Paläontologie, Abhandlungen 183(1–3):391–411.

Hsieh, H.-L. and C.-P. Chen. 2009. Conservation program for the Asian horseshoe crab *Tachypleus tridentatus* in Taiwan: Characterizing the microhabitat of nursery grounds and restoring spawning grounds. In: J.T. Tanacredi, M.L. Botton and D.R. Smith, eds. Biology and Conservation of Horseshoe Crabs. New York: Springer. pp. 417–438.

Jell, P.A. 1989. Some aberrant exoskeletons from fossil and living arthropods. Memoirs of the Queensland Museum 27(2):491–498.

Kaplan, R., S.S.L. Li and J.M. Kehoe. 1977. Molecular characterization of limulin, a sialic acid binding lectin from the hemolymph of the horseshoe crab, *Limulus polyphemus*. Biochemistry 16(19):4297–4303.

Kwan, B.K.Y., H.-L. Hsieh, S.G. Cheung and P.K.S. Shin. 2016. Present population and habitat status of potentially threatened Asian horseshoe crabs *Tachypleus tridentatus* and *Carcinoscorpius rotundicauda* in Hong Kong: A proposal for marine protected areas. Biodiversity and Conservation 25(4):673–692.

Lamsdell, J.C. 2013. Revised systematics of Palaeozoic 'horseshoe crabs' and the myth of monophyletic Xiphosura. Zoological Journal of the Linnean Society 167(1):1–27.

—2016. Horseshoe crab phylogeny and independent colonizations of fresh water: Ecological invasion as a driver for morphological innovation. Palaeontology 59(2):181–194.

Lankester, E.R. 1881. *Limulus* an Arachnid. Quarterly Journal of Microscopical Science 23:504–649.

Latreille, P.A. 1802. Histoire Naturelle, Générale et Particulière, des Crustacés et des Insectes. Paris: F. Dufart. 467 pp. (in French)

Leach, W.E. 1819. Entomostraca. Dictionaire des Science Naturelles. Paris: Levrault and Schoell. 537 pp. (in French)

Linnaeus, C. 1758. Systema Naturæ per Regna Tria Naturæ: Secundum classes, ordines, genera, species, cum characteribus, differentiis, synonymis, locis. 10th edition, Volume 1. Stockholm: Laurentius Salvius. 823 pp. (in Latin)

Lu, Y. 1950. On the genus *Redlichia* with description of its new species. Geological Review 15:157–170. (in Chinese)

Miyata, T., K. Usui and S. Iwanaga. 1984. The amino acid sequence of coagulogen isolated from southeast Asian horseshoe crab, *Tachypleus gigas*. Journal of Biochemistry 95(6):1793–1801.

Müller, O.F. 1785. Entomostraca seu Insecta Testacea, quae in aquis Daniae et Norvegiae reperit, descripsit et iconibus illustravit. Leipzig and Copenhagen: Sumtibus Bibliopolii J.G. Mülleriani. 135 pp. (in Latin)

Nakamura, S., S. Iwanaga, T. Harada and M. Niwa. 1976. A clottable protein (coagulogen) from amoebocyte lysate of Japanese horseshoe crab (*Tachypleus tridentatus*). Its isolation and biochemical properties. Journal of Biochemistry 80(5):1011–1021.

Nelson, B.R., B. Satyanarayana, J.M.H. Zhong, F. Shaharom, M. Sukumaran and A. Chatterji. 2015. Episodic human activities and seasonal impacts on the *Tachypleus gigas* (Müller, 1785) population at Tanjung Selangor in Peninsular Malaysia. Estuarine, Coastal and Shelf Science 164:313–323.

Obst, M., S. Faurby, S. Bussarawit and P. Funch. 2012. Molecular phylogeny of extant horseshoe crabs (Xiphosura, Limulidae) indicates Paleogene diversification of Asian species. Molecular Phylogenetics and Evolution 62(1):21–26.

Owen, A.W. 1985. Trilobite abnormalities. Transactions of the Royal Society of Edinburgh: Earth Sciences 76(2–3):255–272.

Owen, R. 1872. On the anatomy of the American King-crab (*Limulus polyphemus*, Latr.). Transactions of the Linnean Society of London 28(3):459–506.

Pates, S., R.D.C. Bicknell, A.C. Daley and S. Zamora. 2017. Quantitative analysis of repaired and unrepaired damage to trilobites from the Cambrian (Stage 4, Drumian) Iberian Chains, NE Spain. Palaios 32(12):750–761.

Prado, M.C., E. Verneuil and J. Barrande. 1860. Sur l'existence de la faune primordialcdans la Châine Cantabrique. Bulletin de la Société Géologique de France, Series 2 17:516–542. (in French)

Rudkin, D.M. and G.A. Young. 2009. Horseshoe crabs—An ancient ancestry revealed. In: J.T. Tanacredi, M.L. Botton and D.R. Smith, eds. Biology and Conservation of Horseshoe Crabs. Boston: Springer. pp. 25–44.

Selden, P.A. and D.J. Siveter. 1987. The origin of the limuloids. Lethaia 20(4):383–392.

Shultz, J.W. 2001. Gross muscular anatomy of *Limulus polyphemus* (Xiphosura, Chelicerata) and its bearing on evolution in the Arachnida. Journal of Arachnology 29(3):283–303.

Shuster, C.N. 1982. A pictorial review of the natural history and ecology of the horseshoe crab *Limulus polyphemus*, with reference to other Limulidae. Progress in Clinical and Biological Research 81:1–52.

Shuster, C.N., R.B. Barlow and H.J. Brockmann, eds. 2003. The American Horseshoe Crab. Cambridge, MA: Harvard University Press. 472 pp.

Shuster, C.N. and K. Sekiguchi. 2009. Basic habitat requirements of the extant species of horseshoe crabs (Limulacea). In: J.T. Tanacredi, M.L. Botton and D.R. Smith, eds. Biology and Conservation of Horseshoe Crabs. New York: Springer. pp. 115–129.

Sokoloff, A. 1978. Observations on populations of the horseshoe crab *Limulus* (= *Xiphosura*) *polyphemus*. Researches on Population Ecology 19(2):222–236.

Størmer, L. 1952. Phylogeny and taxonomy of fossil horseshoe crabs. Journal of Paleontology 26(4):630–640.

—1955. Merostomata. In: R.C. Moore, ed. Treatise on Invertebrate Paleontology, Part P, Arthropoda 2. Lawrence, KS: University of Kansas, Geological Society of America. pp. 4–41.

van der Meer Mohr, J.C. 1935. Sur quelques malformations chez la limule, *Tachypleus gigas*. Miscellanea Zoologica Sumatrana 87:1–3. (in French)

Van Roy, P., P.J. Orr, J.P. Botting, L.A. Muir, J. Vinther, B. Lefebvre, K. El Hariri and D.E.G. Briggs. 2010. Ordovician faunas of Burgess Shale type. Nature 465(7295):215–218.

Woodward, H. 1879. Contributions to the knowledge of fossil Crustacea. Quarterly Journal of the Geological Society 35(1):549–556.

Higher Degree Research Thesis by Publication
University of New England

STATEMENT OF ORIGINALITY

(To appear at the end of each thesis chapter submitted as an article/paper)

We, the Research Master/PhD candidate and the candidate's Principal Supervisor, certify that the following text, figures and diagrams are the candidate's original work.

Type of work	Page number/s
Scientific publication	129–141

Name of Candidate: Russell D. C. Bicknell

Name/title of Principal Supervisor: John R. Paterson

_____ 11/04/2019
Candidate Date

_____ 11/04/2019
Principal Supervisor Date

Higher Degree Research Thesis by Publication
University of New England

STATEMENT OF AUTHORS' CONTRIBUTION

(To appear at the end of each thesis chapter submitted as an article/paper)

We, the Research Master/PhD candidate and the candidate's Principal Supervisor, certify that all co-authors have consented to their work being included in the thesis and they have accepted the candidate's contribution as indicated in the *Statement of Originality*.

	Author's Name (please print clearly)	**% of contribution**
Candidate	Russell D. C. Bicknell	75
Other Authors	Stephen Pates	25

Name of Candidate: Russell D. C. Bicknell

Name/title of Principal Supervisor: John R. Paterson

_____ 11/04/2019

Candidate Date

_ 11/04/2019

Principal Supervisor Date

Paper 7

Quantitative analysis of repaired and unrepaired damage to trilobites from the Cambrian (Stage 4, Drumian) Iberian Chains, NE Spain

Higher Degree Research Thesis by Publication
University of New England

STATEMENT OF ORIGINALITY

(To appear at the end of each thesis chapter submitted as an article/paper)

We, the Research Master/PhD candidate and the candidate's Principal Supervisor, certify that the following text, figures and diagrams are the candidate's original work.

Type of work	Page number/s
Scientific publication	147–158

Name of Candidate: Russell D. C. Bicknell

Name/title of Principal Supervisor: John R. Paterson

Candidate — 11/04/2019 Date

Principal Supervisor — 11/04/2019 Date

Higher Degree Research Thesis by Publication
University of New England

STATEMENT OF AUTHORS' CONTRIBUTION

(To appear at the end of each thesis chapter submitted as an article/paper)

We, the Research Master/PhD candidate and the candidate's Principal Supervisor, certify that all co-authors have consented to their work being included in the thesis and they have accepted the candidate's contribution as indicated in the *Statement of Originality*.

	Author's Name (please print clearly)	**% of contribution**
Candidate	Russell D.C. Bicknell	25
Other Authors	Stephen Pates	55
	Allison C. Daley	10
	Samuel Zamora	10

Name of Candidate: Russell D. C. Bicknell

Name/title of Principal Supervisor: John R. Paterson

_____ 11/04/2019
Candidate Date

_____ 11/04/2019
Principal Supervisor Date

Paper 8

Elongated thoracic spines as potential predatory deterrents in olenelline trilobites from the lower Cambrian of Nevada

Higher Degree Research Thesis by Publication
University of New England

STATEMENT OF ORIGINALITY

(To appear at the end of each thesis chapter submitted as an article/paper)

We, the Research Master/PhD candidate and the candidate's Principal Supervisor, certify that the following text, figures and diagrams are the candidate's original work.

Type of work	Page number/s
Scientific publication	163–174

Name of Candidate: Russell D. C. Bicknell

Name/title of Principal Supervisor: John R. Paterson

_____ 11/04/2019
Candidate Date

_____ 11/04/2019
Principal Supervisor Date

Higher Degree Research Thesis by Publication
University of New England

STATEMENT OF AUTHORS' CONTRIBUTION

(To appear at the end of each thesis chapter submitted as an article/paper)

We, the Research Master/PhD candidate and the candidate's Principal Supervisor, certify that all co-authors have consented to their work being included in the thesis and they have accepted the candidate's contribution as indicated in the *Statement of Originality*.

	Author's Name (please print clearly)	**% of contribution**
Candidate	Russell D.C. Bicknell	25
Other Authors	Stephen Pates	75

Name of Candidate: Russell D. C. Bicknell

Name/title of Principal Supervisor: John R. Paterson

_____ 11/04/2019
Candidate Date

_____ 11/04/2019
Principal Supervisor Date

Supplementary Papers

The supplementary papers represent contributions to research by the candidate that were completed during the candidature, but are not included in assessment for the Ph.D. thesis (first pages only are included).

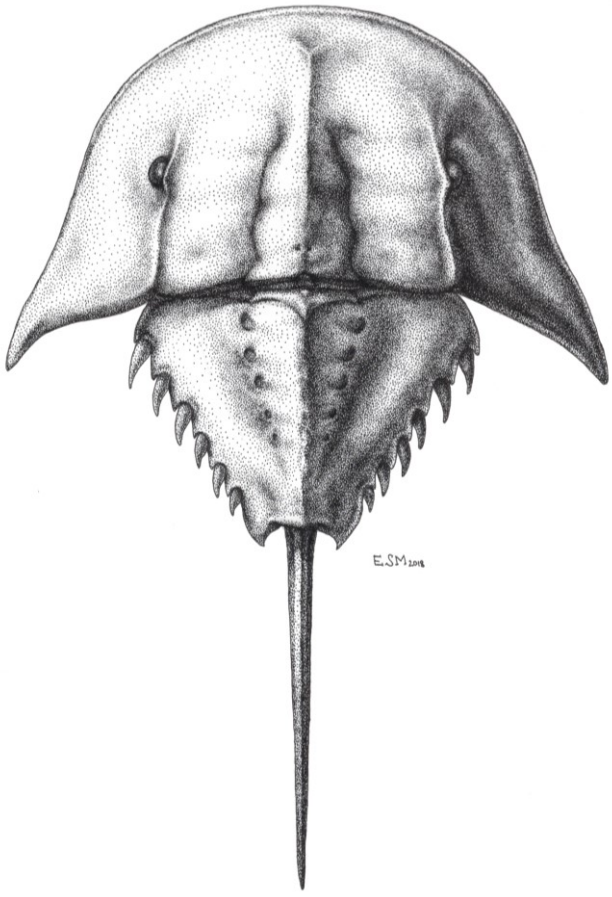

Reconstruction of Sloveniolimulus rudkini*, the first fossil horseshoe crab from the Triassic of Slovenia (Described in Paper 12). Illustration by E. Martin.*

ORIGINAL ARTICLE

WILEY Acta Zoologica

Cuticular microstructure of Australian ant mandibles confirms common appendage construction

Molly M. Barlow[1] | **Russell D. C. Bicknell**[2] | **Nigel R. Andrew**[1]

[1]School of Environmental and Rural Science, University of New England, Armidale, New South Wales, Australia

[2]Palaeoscience Research Centre, School of Environmental and Rural Science, University of New England, Armidale, New South Wales, Australia

Correspondence
Russell D. C. Bicknell, Palaeoscience Research Centre, School of Environmental and Rural Science, University of New England, Armidale, NSW, Australia.
Email: rdcbicknell@gmail.com

Funding information
Australian Postgraduate Award (RDCB); Australian Research Council Discovery Project Award, Grant/Award Number: DP160101561

Abstract

Exoskeletons characterise Arthropoda and have allowed the morphological and taxonomic diversity of the phylum. Exoskeletal sclerotisation occurs in genetically designated regions, and mandibles represent one such area of high sclerotisation. Mandible morphology reflects dietary preferences and niche partitioning and has therefore been well documented. However, mandibular cuticular microstructure has been under-documented. Here we use scanning electron microscopy to explore mandible microstructure in four disparate Australian Formicidae taxa (ants) with different life modes and diets: *Camponotus nigriceps*, *Iridomyrmex purpureus*, *Odontomachus simillimus* and *Rhytidoponera aciculata*. We test the hypothesis that mandible construction is highly conserved across these species, as would be expected for arthropod cuticle. We show broadly similar mandible microstructure but report that pore canals and cuticular indentations are not ubiquitous among all studied taxa. Our preliminary results demonstrate that ant taxa have morphologically plastic mandibles with a highly conserved construction, potentially reflecting an interesting record of evolutionary stasis.

KEYWORDS

ants, arthropoda, Australia, *Camponotus nigriceps*, cuticular microstructure, *Iridomyrmex purpureus*, mandibles, *Odontomachus simillimus*, *Rhytidoponera aciculata*

1 | INTRODUCTION

Arthropods represent one of the most species-rich groups with between 2.9–12.7 million extant species, accounting for ca. 80% of animal biodiversity (Hamilton et al., 2013; Rota-Stabelli et al., 2011). The arthropod exoskeleton provides shape, rigidity and protection against predators and allowed the group to diversify across the Phanerozoic. The exoskeletal cuticle is secreted from epidermal cells during ecdysis and consists of a thin (1–4 μm) epicuticle layer (Mani, 1973) and the thicker (10–100 μm) procuticle (Chen, Peng, Wang, Zhang, & Zhang, 2002; Muzzarelli, 2011). Procuticle is divided into a sclerotised exocuticle—hardened and darkened cuticle (Richards & Davies, 1977)—and a softer, more elastic endocuticle (Chen et al., 2002; Muzzarelli, 2011). The degree of sclerotisation varies across the exoskeleton, and mandibles—modified anterior appendages that characterise Mandibulata—are often highly sclerotised regions (Edgecombe, Richter, & Wilson, 2003; Vincent & Wegst, 2004). The highly sclerotised nature of mandibles means that they are used in fighting, food manipulation, and larvae nesting (Fabritius et al., 2011; Patterson, 1984; Wheeler, 1926). These are all applications that produce variable intra- and inter-taxon mandible morphology (Fabritius et al., 2011; Manting, Torres, & Demayo, 2015).

Hymenoptera is a large and diverse insect group with taxa exhibiting a range of mandible morphologies (Keller, 2011). External morphology of ant (Hymenoptera: Formicidae) mandibles is thoroughly documented (Cribb et al., 2008; Da Silva Camargo, Hastenreiter, Forti, Lopes, & Floriano, 2015;

SCIENTIFIC REPORTS

OPEN

Rheotaxis in the Ediacaran epibenthic organism *Parvancorina* from South Australia

Received: 15 November 2016
Accepted: 27 February 2017
Published: 30 March 2017

John R. Paterson[1], James G. Gehling[2], Mary L. Droser[3] & Russell D. C. Bicknell[1]

Diverse interpretations of Ediacaran organisms arise not only from their enigmatic body plans, but also from confusion surrounding the sedimentary environments they inhabited and the processes responsible for their preservation. Excavation of Ediacaran bedding surfaces of the Rawnsley Quartzite in South Australia has provided the opportunity to study the community structure of the Ediacara biota, as well as the autecology of individual organisms. Analysis of two bedding surfaces preserving large numbers of *Parvancorina* illustrates that individuals display a preferred, unidirectional orientation aligned with current, as indicated by the identified current proxies: tool marks, overfolded edges of *Dickinsonia*, felled fronds and drag structures generated by uprooted frond holdfasts. Taphonomic and morphological evidence suggests that the preferred orientations of *Parvancorina* individuals are not the result of passive current alignment, but represent a rheotactic response at some stage during their life cycle. These results illustrate a previously unrecognized life mode for an Ediacaran organism and arguably the oldest known example of rheotaxis in the fossil record. The morphology and previously suggested phylogenetic affinities of *Parvancorina* are also re-evaluated. Apart from possessing a bilaterally symmetrical body, there are no unequivocal morphological characters to support placement of *Parvancorina* within the Euarthropoda or even the Bilateria.

Body fossil evidence that shows the ability of Ediacaran organisms to physically respond to external stimuli or move within their environment is generally rare[1]. The only broadly accepted evidence of motility and associated behaviours in the Ediacara biota is represented by trace fossils from Canada, China, Namibia, Russia, and South Australia[2–6]. Previous attempts to compare Ediacara disc-shaped fossils (e.g., *Aspidella*) with free-swimming medusoids have been discounted in light of evidence that these were either attachment discs for frond-like organisms[7] or a motile, benthic animal of cnidarian grade[8]. Serial imprints left by flat organisms such as *Dickinsonia* and *Yorgia* have been previously interpreted as multiple decayed organisms or touch-down impressions made by current-shuffled individuals, but they are likely evidence of periodic creeping to feed via adsorption of mat nutrients[9–13]. This last interpretation is based on examples that show an external mould of a body fossil at the end of a serial set of faint, similar-sized casts, aligned such that the presumed anterior end of the organism is most distant from the chain of body imprints. There is also evidence of grazing and locomotory traces associated with body fossils of *Kimberella*[14,15], and even signs of possible tactophobic behaviour in *Dickinsonia*[11]. Here we report new information on the problematic Ediacaran organism *Parvancorina minchami* from two bed assemblages of the Rawnsley Quartzite in South Australia, suggesting that this taxon was capable of performing rheotaxis—oriented movement or positioning in response to a water current—during at least part of its life cycle.

Results

Bed assemblages. Specimens of *Parvancorina* were examined on two separate beds, Parv Bed and MM3, of the Ediacara Member of the Rawnsley Quartzite at Nilpena, Flinders Ranges, South Australia[16] (Fig. 1). Parv Bed is a part of the 'Planar-Laminated and Rip-Up Sandstone Facies' that represents sub-wave base upper canyon fill deposited as unidirectional sheet-flow sands, whereas MM3 exemplifies the 'Oscillation-Rippled Sandstone Facies', which is interpreted to have been deposited between fair-weather and storm wave base[17]. These beds have been excavated, inverted and reassembled to study the fossil assemblages on the bed soles. On both beds,

[1]Palaeoscience Research Centre, School of Environmental and Rural Science, University of New England, Armidale, NSW 2351, Australia. [2]South Australian Museum, North Terrace, Adelaide, SA 5000, Australia. [3]Department of Earth Sciences, University of California, Riverside, California 92521, USA. Correspondence and requests for materials should be addressed to J.R.P. (email: jpater20@une.edu.au)

iScience

CellPress

Article

Evolutionary Transition in the Late Neogene Planktonic Foraminiferal Genus *Truncorotalia*

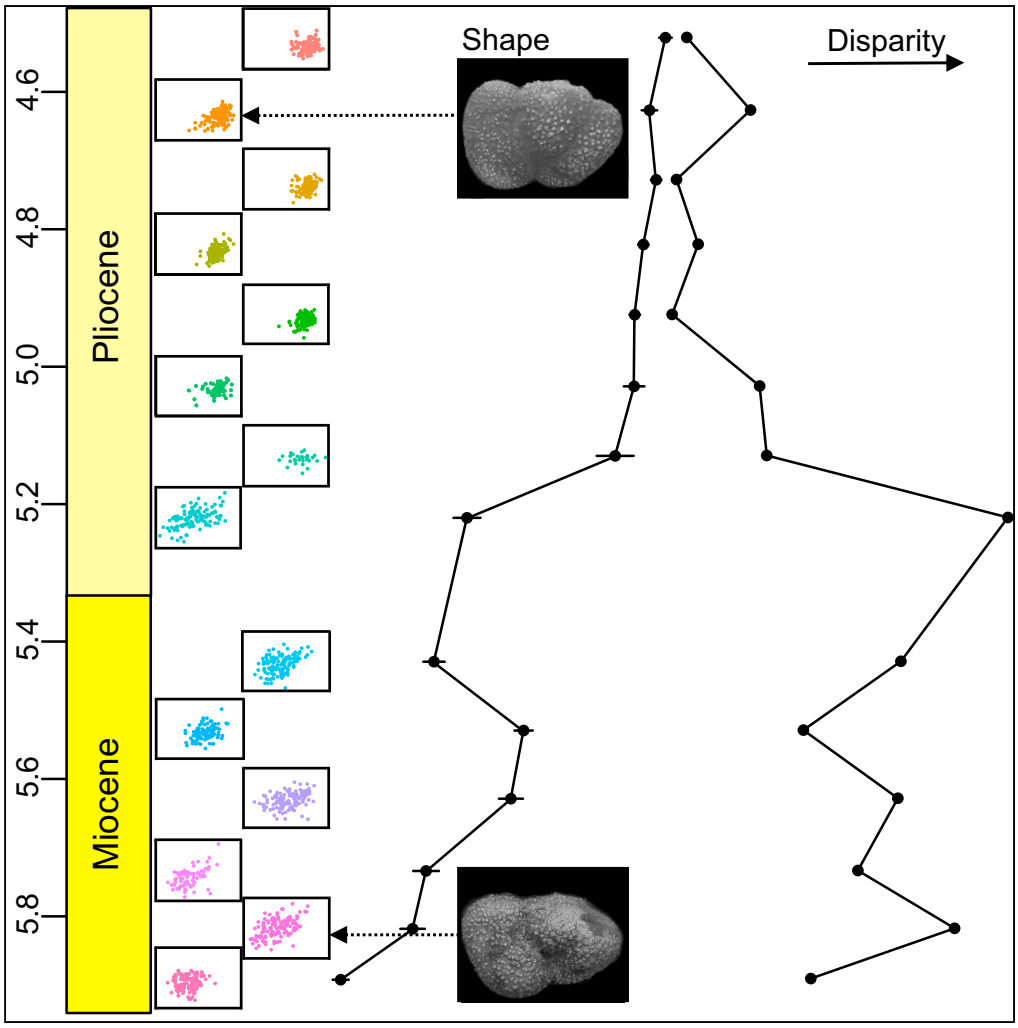

Russell D.C. Bicknell, Katie S. Collins, Martin Crundwell, Michael Hannah, James S. Crampton, Nicolás E. Campione

rdcbicknell@gmail.com

HIGHLIGHTS

Evolution of planktonic foraminiferal anatomy across Miocene/Pliocene boundary

Novel application of multivariate analyses to 1,459 specimens

Evidence for a punctuated anatomical shift associated with the boundary

Bicknell et al., iScience ■■, 1–9
■■, 2018
https://doi.org/10.1016/j.isci.2018.09.013

Geological Magazine

www.cambridge.org/geo

A new limulid genus from the Strelovec Formation (Middle Triassic, Anisian) of northern Slovenia

Russell D. C. Bicknell[1,*], Jure Žalohar[2], Primož Miklavc[3], Bogomir Celarc[4], Matija Križnar[5] and Tomaž Hitij[6]

[1]Palaeoscience Research Centre, School of Environmental and Rural Science, University of New England, Armidale, 2351, Australia; [2]T-TECTO, Koroška cesta 12, SI-4000 Kranj, Slovenia; [3]Department of Geology, Faculty of Natural Sciences and Engineering, University of Ljubljana, Aškerčeva ceta 12, SI-1000 Ljubljana, Slovenia; [4]Geological Survey of Slovenia, Dimičeva ulica 14, SI–1000 Ljubljana, Slovenia; [5]Slovenian Museum of Natural History, Prešernova 20, SI-1000 Ljubljana, Slovenia and [6]Dental School, Faculty of Medicine, University of Ljubljana, Hrvatski trg 6, SI-1000 Ljubljana, Slovenia

Original Article

Cite this article: Bicknell RDC, Žalohar J, Miklavc P, Celarc B, Križnar M, and Hitij T. A new limulid genus from the Strelovec Formation (Middle Triassic, Anisian) of northern Slovenia. *Geological Magazine* https://doi.org/10.1017/S0016756819000323

Received: 30 October 2018
Revised: 11 March 2019
Accepted: 19 March 2019

Keywords:
Triassic; Strelovec Formation; Xiphosurida; horseshoe crab; Limulidae; *Sloveniolimulus*; Slovenia; geometric morphometrics

Author for correspondence:
Russell D. C. Bicknell,
Email: rdcbicknell@gmail.com

Abstract

Horseshoe crabs are an archetypal chelicerate group with a fossil record extending back to Early Ordovician time. Although extensively studied, the group generally has a low diversity across the Phanerozoic Eonothem. Here, we expand the known diversity of true horseshoe crabs (Xiphosurida) by the description of a new taxon from the Middle Triassic Strelovec Formation of the Slovenian Alps. The mostly complete fossil is preserved as an external mould and assigned to the family Limulidae Zittel, 1881 as *Sloveniolimulus rudkini*, n. gen., n. sp. The use of landmark and semilandmark geometric morphometrics is explored to corroborate the systematic palaeontology and suggests that the new genus and species are valid. We also provide the first quantitative evidence for the extensive diversity of Triassic horseshoe crabs. We suggest that Triassic horseshoe crabs likely filled many ecological niches left vacant after the end-Permian extinction.

1. Introduction

Horseshoe crabs are iconic chelicerates that have been extensively studied by both biologists and palaeontologists. Extant taxa have been subject to detailed anatomical (Owen, 1872; Lankester, 1881; Shultz, 2001; Bicknell et al. 2018*a*, *c*, *d* Bicknell & Pates, 2019), biochemical (Kaplan *et al.* 1977), biomechanical (Bicknell *et al.* 2018*b*), ecological (Sokoloff, 1978; Shuster Jr, 1982; Shuster Jr & Sekiguchi, 2009; Fairuz-Fozi *et al.* 2018) and genetic (Sokoloff, 1978; Obst *et al.* 2012) studies. Palaeontological interest in horseshoe crabs stems from the extensive xiphosuran fossil record from Early Ordovician time to today (Van Roy *et al.* 2010, 2015), and the observation that Mesozoic crown-group horseshoe crabs (Xiphosurida) are morphologically similar to extant species, such that two extant genera have fossil records extending back to Triassic time (Błażejowski, 2015; Lamsdell & McKenzie, 2015; Błażejowski *et al.* 2016). The morphological similarity has been used to illustrate delayed evolution (Fisher, 1984) and stunning morphological conservation over at least 148 Ma (Avise *et al.* 1994; Rudkin & Young, 2009; Kin & Błażejowski, 2014; Bicknell *et al.* 2018*d*). Despite extensive study, Mesozoic horseshoe crab diversity is low (Fisher, 1982, 1984) with only 13 genera, known mostly from the Triassic Period (Fig. 1). These are the extinct genera *Austrolimulus*, *Limulitella*, *Mesolimulus*, *Paleolimulus*, *Psammolimulus*, *Tarracolimulus*, *Vaderlimulus*, and *Yunnanolimulus*, and two extant genera *Limulus* and *Tachypleus* (Dunlop *et al.* 2018). The number of genera reflects either a limited diversity or the requirement for exceptional preservation in *Konservat-Lagerstätten* to preserve the xiphosurid cuticular exoskeleton (Babcock & Merriam, 2000; Babcock *et al.* 2000). Here, we increase the Triassic horseshoe crab diversity by presenting the first exceptionally preserved horseshoe crab from a Middle Triassic *Konservat-Lagerstätte* in northern Slovenia. To our best knowledge, this is the only horseshoe crab fossil reported from an alpine Triassic deposit. We also pioneer geometric morphometrics as a tool for horseshoe crab research to show where the new specimen is located in morphospace relative to 48 horseshoe crab specimens that range from the Carboniferous Period to today.

2. Geological history and setting

The investigated horseshoe crab fossil was found in the Strelovec Formation (Fig. 2) in the Kamnik-Savinja Alps on the northern slopes of the Križevnik Mountain (1909 m) in the Robanov Kot Valley (Fig. 3). The Kamnik-Savinja Alps are located in northern Central

CAMBRIDGE UNIVERSITY PRESS

CONCLUSION AND FUTURE DIRECTIONS

Prior to the work presented within this thesis, our understanding of Cambrian predator-prey systems was somewhat hypothetical. The effectiveness of Cambrian predators was entirely unknown, use of modern analogues to further understand Cambrian prey injuries was poorly explored, and patterns of predation had not been thoroughly considered since the 1990s. The eight publications, including a literature review summarising state of Cambrian shell-crushing and shell-drilling predation, have advanced knowledge on these topics. They have been instrumental in developing new applications of modern analogues in Cambrian invertebrate palaeontology. While conducting these studies, important future research directions presented themselves.

The effectiveness of Cambrian gnathobase-bearing predators was a topic that plagued the literature prior to the results presented in Papers 2–4, and there was little definitive evidence to support any hypotheses in the topic. Papers 2 and 4 revealed how well Cambrian gnathobases, at least for *Sidneyia inexpectans*, were built for shell crushing and showed that a gnathobasic toolkit was a biomechanically-effective form of durophagous predation over 500 million years ago. Furthermore, for researchers interested in the biomechanical modelling of Cambrian animals, Papers 3 and 4 presented a novel methodology with which to explore this topic. While the use of Finite Element Analyses (FEA) was successful in documenting the mechanical advantage of extinct gnathobase-bearing arthropods, protopodal gnathobases were not employed by the most iconic predatory Cambrian arthropods: the radiodonts. This group primarily used their frontal appendages and oral cones to possibly crush and consume prey (Whittington & Briggs, 1985; Babcock & Robison, 1989; Nedin, 1999; Liu et al., 2018), with some groups potentially employing gnathobase-like structures on the reduced neck segments close to the anterior head region (Cong et al., 2017, 2018). It is possible that a 3D

biomechanical method related to FEA—Multi-Body Dynamic Analysis (Bates & Falkingham, 2012; Snively et al., 2013)—may uncover how effective radiodonts were at predation and further the understanding of feeding habits in Cambrian predators.

The use of extant arthropods to inform how fossil groups may have experienced, and recovered from injuries has been rarely considered (Conway Morris & Jenkins, 1985; Jell, 1989). As such, groups such as horseshoe crabs have not been explicitly used to understand how trilobite injuries developed. Papers 5 and 6 highlighted that extreme cephalic injuries on Cambrian trilobites occurred after a moulting event and select thoracic abnormalities reflect abnormal recovery after an injury. An extension of this work, as suggested in Paper 6, would be to induce damage to the exoskeletons of living horseshoe crabs in the lab and document how they recover from injuries during subsequent moulting events. This type of research would not inflict pain on the organism as the chitinous exoskeleton is not connected to the nervous system of the animal. These data can then be applied to trilobites to suggest how they may have recovered from injuries.

Finally, Cambrian trilobite injuries and associated predator-prey dynamics have not been documented in-depth, or statistically, since Babcock (1993). As such, Papers 7 and 8 presented important steps towards revising this topic and better understanding this hallmark of the Cambrian Explosion. The key advancement was the realisation that by considering a single deposit and taxon in isolation, true patterns of injuries can be uncovered. The main outcomes were that right-sided injuries are not ubiquitous across the Cambrian and injuries are commonly posteriorly located. In conducting this work, it was realised that other deposits with injured specimens need to be revisited to further confirm the lack of injury lateralisation. These include the Emu Bay Shale (Cambrian Series 2, Stage 4), Australia (Conway Morris & Jenkins, 1985; Daley et al., 2013) and the Jince Formation (Miaolingian Series, Drumian), Czech Republic (Šnajdr, 1978; Fatka et al., 2008, 2015), both of which have injured

specimens. Furthermore, documented injuries from Cambrian species could be compiled to revise and build on Owen (1985): a seminal work on trilobite abnormalities.

References

Babcock, L. E. (1993). Trilobite malformations and the fossil record of behavioral asymmetry. *Journal of Paleontology, 67*, 217–229.

Babcock, L. E., & Robison, R. A. (1989). Preferences of Palaeozoic predators. *Nature, 337*, 695–696.

Bates, K. T., & Falkingham, P. L. (2012). Estimating maximum bite performance in *Tyrannosaurus rex* using multi-body dynamics. *Biology Letters*, rsbl20120056.

Cong, P., Daley, A. C., Edgecombe, G. D., & Hou, X. (2017). The functional head of the Cambrian radiodontan (stem-group Euarthropoda) *Amplectobelua symbrachiata*. *BMC Evolutionary Biology, 17*, 208.

Cong, P., Edgecombe, G. D., Daley, A. C., Pates, S., & Hou, X. (2018). New radiodontans with gnathobase-like structures from the Cambrian Chengjiang Biota and implications for the systematics of Radiodonta. *Papers in Palaeontology, 4*, 605–621.

Conway Morris, S., & Jenkins, R. J. F. (1985). Healed injuries in early Cambrian trilobites from South Australia. *Alcheringa, 9*, 167–177.

Daley, A. C., Paterson, J. R., Edgecombe, G. D., García-Bellido, D. C., & Jago, J. B. (2013). New anatomical information on *Anomalocaris* from the Cambrian Emu Bay Shale of South Australia and a reassessment of its inferred predatory habits. *Palaeontology, 56*, 971–990.

Fatka, O., Budil, P., & Grigar, L. (2015). A unique case of healed injury in a Cambrian trilobite. *Annales de Paléontologie, 101*, 295–299.

Fatka, O., Szabad, M., Budil, P., & Micka, V. (2008). Position of trilobites in Cambrian ecosystem: Preliminary remarks from the Barrandian region (Czechia). *Advances in Trilobite Research, 9*, 117–121.

Jell, P. A. (1989). Some aberrant exoskeletons from fossil and living arthropods. *Memoirs of the Queensland Museum, 27*, 491–498.

Liu, J., Lerosey-Aubril, R., Steiner, M., Dunlop, J. A., Shu, D., & Paterson, J. R. (2018). Origin of raptorial feeding in juvenile euarthropods revealed by a Cambrian radiodontan. *National Science Review, 5*, 863–869.

Nedin, C. (1999). *Anomalocaris* predation on nonmineralized and mineralized trilobites. *Geology, 27*, 987–990.

Owen, A. W. (1985). Trilobite abnormalities. *Transactions of the Royal Society of Edinburgh: Earth Sciences, 76*, 255–272.

Šnajdr, M. (1978). Anomalous carapaces of Bohemian paradoxid trilobites. *Sborník Geologických Věd Paleontologie, 20*, 7–31.

Snively, E., Cotton, J. R., Ridgely, R., & Witmer, L. M. (2013). Multibody dynamics model of head and neck function in *Allosaurus* (Dinosauria, Theropoda). *Palaeontologia Electronica, 16*, 1–29.

Whittington, H. B., & Briggs, D. E. G. (1985). The largest Cambrian animal, *Anomalocaris*, Burgess Shale, British Columbia. *Philosophical Transactions of the Royal Society of London. B, Biological Sciences, 309*, 569–609.